Clays and Clay Minerals, Vol. 52, No. 5, 552–575, 2004.

HETEROGENEOUS MIXED-LAYER CLAYS FROM THE CRETACEOUS GREENSAND, ISLE OF WIGHT, SOUTHERN ENGLAND

DOUGLAS K. MCCARTY[1,*], VICTOR A. DRITS[2], BORIS SAKHAROV[2], BELLA B. ZVIAGINA[2], ALASTAIR RUFFELL[3] AND GRANT WACH[4]

[1] ChevronTexaco, 3901 Briarpark, Houston, TX 77063, USA
[2] Geological Institute of the Russian Academy of Science, Pyzevskij per. D.7, 119017 Moscow, Russia
[3] Queen's University, Belfast, UK
[4] Dalhousie University, Halifax, N.S., BJ3 3J5 Canada

Abstract—The sea-cliffs of the Isle of Wight were deposited during a period of overall sea-level rise starting in the Barremian (Lower Cretaceous) and continuing into the Aptian and Albian. They consist of fluvial, coastal and lagoonal sediments including greensands and clays. Numerous episodes of erosion, deposition and faunal colonization reflect condensation and abandonment of surfaces with firmgrounds and hardgrounds. This study focused mainly on shallow marine cycles where variations in clay mineralogy would not be expected, because overall system composition, sediment source, and thermal history are similar for all the samples in the studied section. Instead we found a wide variety of clay assemblages even in single samples within a 200 m interval.

In this interval, distinct clay mineral assemblages were found and can be described as consisting of Al-rich, Fe-rich and intermediate Fe and Al compositions with respect to 2:1 and 1:1 layers in mixed-layer arrangements. Nearly pure glauconite-nontronite clays exist in the <2 μm fraction only when the bulk rock is free of K- and plagioclase feldspar. Conditions favorable to glauconite-nontronite formation are interpreted to result from a hiatus in volcanoclastic sedimentation, thus providing a stable substrate for glauconitization.

The Fe-bearing mixed-layer clay assemblages consist of glauconite, nontronite and berthierine-like layers in various proportions with several mixed-layer clays often coexisting in the same sample. In different samples, Al-rich and Fe-Mg-rich mixed-layer clays are similar in their content and distribution of 1:1 and 2:1 layers. This suggests that the original clay assemblages were similar and later diagenesis affected certain horizons resulting in substitution of Al by Fe + Mg while preserving the original layer structure and arrangement.

Structural formulae for the berthierine-like phase and berthierine-like layers in these mixed-layer clays show their layer cation composition is intermediate between odinite and standard berthierine. The total sum of octahedral cations varies from 5.26 to 5.55 whereas the amount of Fe^{2+} cations varies from 2.12 to 2.22 per $O_{10}(OH)_8$. A feature of the berthierine-like phase as well as of berthierine-like layers is that they are di-trioctahedral and Fe^{2+} and Fe^{3+} are the prevalent cations. Moreover, in these berthierine-like components, the amount of Fe^{2+} is greater than that of Mg (in contrast to odinite) and Fe^{3+} cations prevail over Al (in contrast to berthierine). The presence of authigenic ferrous Fe clays and the relationship between glauconite-nontronite and bulk mineralogy has implications for sedimentological processes and geochemical conditions during and shortly after deposition.

Key Words—Berthierine, Cretaceous. Glauconite, Isle of Wight, Heterogeneous Mixed-layer Clays, Nontronite.

INTRODUCTION

The Cretaceous strata exposed in the sea cliffs of the Isle of Wight (Figure 1) were deposited during a period of overall sea-level rise that began during deposition of Barremian (Lower Cretaceous) fluvial, coastal and lagoonal sediments. Similar glauconitic and bentonite-bearing sandstone and mudstone deposits extend throughout southern England (Figure 1) and thence into the North Atlantic, North Sea and Germany. As the marine transgression continued into the Aptian and Albian, greensands and clays were deposited (Ruffell and Wach, 1991). Equivalent-age greensands form important oil and gas reservoirs in the Celtic Sea and North Sea. Prior to the final episode of marine inundation, a succession of tidally-influenced estuarine and baymouth sands and clays occur followed by marine clays and Upper Cretaceous chalk (a coccolith limestone). Throughout this transgression, sediment cyclicity is evident as meter-thick sand-clay alternations or as episodes of non-deposition, firmground/hardground formation and faunal colonization (Ruffell and Wach, 1998).

Sand-clay alternations and cemented firmground horizons on the meter to decimeter scale form potential internal barriers to hydrocarbon flow. Equivalent-age greensands throughout southern England (Figure 1) and beyond in the North Celtic Sea and North Sea contain

* E-mail address of corresponding author:
dmccarty@chevrontexaco.com
DOI: 10.1346/CCMN.2004.0520503

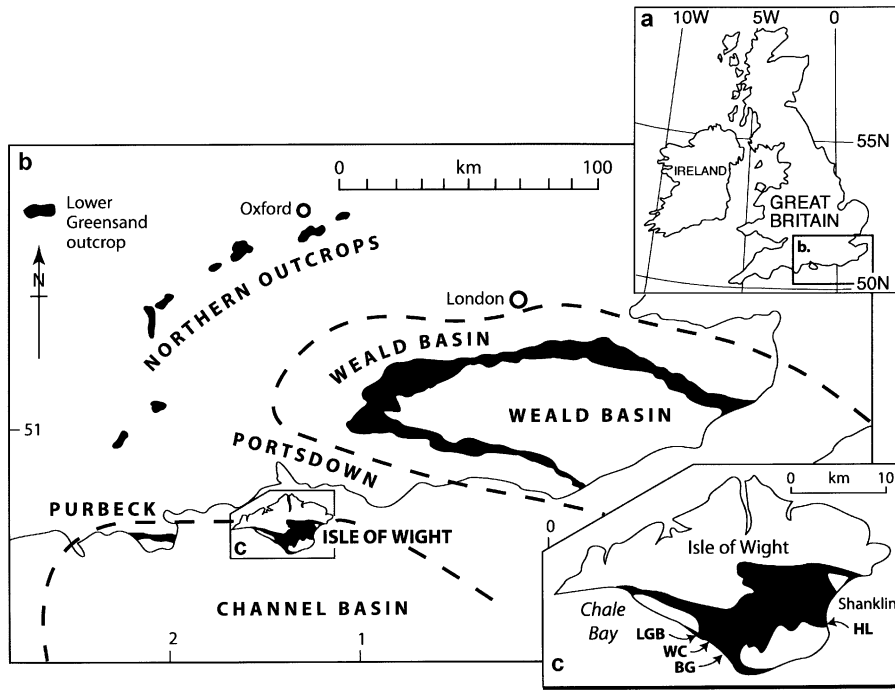

Figure 1. Map of the Isle of Wight and approximate sample locations.

valuable resources. Onshore, contiguous greensands form a major aquifer and contain extensively-mined quartzose sands (for glass manufacture) and bentonite Fuller's Earth seams. Offshore, similar-age and facies sandstones form important oil and gas reservoirs (Celtic Sea and North Sea). Our study examines the clay mineralogy across five such sediment cycles. The first cycle comprises a coarsening-up sandstone unit within coastal and lagoonal mudstones and shales deposited during the initial, non-marine phase of the transgression (Yoshida *et al*., 2001) in the Vectis Formation (Wealden Group). Here, 2–15 m thick quartzose and feldspathic fine to medium-grained sandstones with trough cross-stratification and a ripple-marked top surface are overlain abruptly by gray silty mudstones with an abundant non-marine bivalve fauna.

The next three cycles comprise cemented horizons within the shallow marine Ferruginous Sands (Lower Greensand Group). These represent the firmgrounds documented by Ruffell and Wach (1998) who suggested their origin as episodes of sediment starvation, faunal colonization and storm reworking. The beds are bioturbated, glauconitic and fossiliferous.

The fifth and topmost cycle we examined forms one of three to four dm-thick alternations of green-black bioturbated silty clays and white to green cross-stratified and clay-draped quartzose sands in the Sandrock Formation (Lower Greensand Group). Tidal influence is very apparent in these beds: the lack of ammonite fauna indicates limited marine influence in an estuarine environment of deposition.

Thus our sample sets include strata of coastal, lagoonal and estuarine origin but concentrate on shallow marine cycles where variations in clay mineralogy would not be expected, because overall system composition, sediment source and thermal history are similar for all the samples in the studied section. Instead we found a wide variety of clay assemblages even in single samples within this 200 m interval. A total of 33 samples from these five stratigraphic units were collected and analyzed (Figure 2). The five units, from the bottom, include: Wealden – Barnes High (BH: coastal-lagoonal delta advance), Lower Greensand – Lower Gryphea Bed (LGB), Whale Chine (WC), Horse Ledge (HL) (all shallow-marine firmground non-depositional cycles), and Blackgang (BG: tidal estuarine to shelf).

Unit BH was deposited in a brackish environment, as shown by lack of marine fauna (Ruffell and Wach, 1998). It comprises a 15 m thick (max) overall coarsening-up sandstone with heterolithic silty clay-sandstone beds (1 mm–5 cm thick) in the lower 5–10 m, overlain by cross-stratified sandstones with occasional clay drapes. The BH unit is interpreted as a delta that prograded into a lagoonal or interdistributary bay/estuarine environment prior to the transgression (Ruffell and Wach, 1998). The BH samples were taken from a sandstone-silty clay succession at the top of the siliciclastic deposits that is interpreted to be an estuarine environment.

Units LGB, WC and HL were deposited in a marine environment and can be described together. The sediments are highly bioturbated, cross-stratified sandstones

https://doi.org/10.1346/CCMN.2004.0520503 Published online by Cambridge University Press

interspersed with fossiliferous and non-fossiliferous zones, in addition to glauconitic beds (Ruffell and Wach, 1998). Unit BG comprises white, quartzose and occasionally richly glauconitic sandstones, probably deposited as a succession of tidal sandwaves, baymouth bars and barriers within a large (20 km wide) inlet. Black to green silty clays were probably deposited when channels and inlets were abandoned or when tidal energy was focused elsewhere.

Even though these intervals have similar depositional environments they have significant differences in clay minerals. In some cases, a given clay assemblage may reflect the prevailing depositional conditions, while others may be due to micro-conditions related to biological activity. Some clay types may have formed by weathering in the outcrop, which complicates interpretation of authigenic clay mineral reactions in the depositional setting or subsurface. However, it is clear that for some samples, especially glauconitic and nontronitic types, those sedimentary processes such as sedimentation rate and substrate stability can be inferred. The presence of 1:1 layer clays containing ferrous iron indicates reducing or micro-reducing conditions during clay formation. This section has not been buried to more than 1 km depth and thus deep burial diagenesis can be ruled out (Bray *et al*., 1998).

MATERIALS AND METHODS

The initial objectives of the study were to test surfaces and strata within marginal-marine and shallow marine depositional settings that could form baffles and barriers to flow. The sampling protocol that was developed emphasized these intervals and 33 samples were collected from Isle of Wight outcrops. The reservoir sands were not methodically sampled.

X-ray diffraction (XRD)

Quantitative X-ray diffraction (QXRD). Quantitative X-ray diffraction was conducted on bulk samples following the procedure of Środoń *et al*. (2001). This QXRD technique uses an internal standard (Chung, 1974) and directly calculates the individual mineral phases and clay mineral families without normalization.

Clay-size, oriented aggregate sample analysis. The <2.0 μm equivalent spherical diameter size fraction was separated from samples by standard centrifugation methods. The samples selected for detailed study were treated to remove carbonate and Fe oxide cements with Na acetate buffer and Na dithionite, respectively (Jackson, 1985). The Na^+-saturated clays were exchanged with Ca^{2+} using calcium cation exchange resin beads. Approximately 250 mL of <2.0 μm suspension were shaken overnight with ~5 g of Dowex HCR-W2 resin beads. The suspension was then dried and oriented aggregates were made by evaporation onto glass slides to provide a sample ~4 cm long with at least 10 mg of clay per cm^2 (Moore and Reynolds, 1997). Diffraction scans for each sample were collected using a Scintag X1 diffractometer equipped with a solid-state Si detector, after ethylene glycol (EG) treatment by vapor solvation in a heated (60ºC) chamber and also the ambient (air-dried) state. The scans were made from 2 to 52º2θ with a 0.02º2θ step increment and counting rate of 4 s per step or longer using CuKα radiation transmitted through a 2.0 mm divergence and 4 mm scatter slit. Detector slits were 0.5 mm and 0.2 mm.

A number of papers by Drits and co-workers (*e.g.* Drits *et al*., 1997a,b) demonstrate that clay assemblages in mudstones are heterogeneous and can contain more than one mixed-layer mineral having the same or different types of layers. Often they are three-component mixed-layer types having 2:1 layers with variable charge density and different thickness. Full pattern computer simulation is probably the most effective way to reveal the structural details of such complex mixtures (*e.g.* Drits *et al*., 1997, 2002; Sakharov *et al*., 1999). This technique was used to describe representative samples from Isle of Wight.

In the following, I, GL, S, NR and V denote illite, glauconite, smectite, nontronite and vermiculite-like interlayers or layers, respectively, and GL-NR a mixed-layer glauconite-nontronite. Berthierine-like layers in mixed-layer minerals are denoted as Br. We define layers which in the ethylene glycol solvated state swell to 16.6−16.9 Å and to 12.9−13.5 Å as smectite and vermiculite or high-charge smectite, respectively.

Layer susceptibility to acid was evaluated on selected samples by placing ~200 mg of clay in ~20 mL of 80ºC 1 N HCl for 2 h and periodically stirred. The treated sample was concentrated and cleaned by dialysis for 24 h. The washed clay was then dried and standard mounts were prepared on glass slides and diffraction data were collected as for the air-dried and EG solvated samples.

Clay-size, random powder analysis. Random powder diffraction data were obtained from the <2.0 μm size fraction of selected samples after freeze drying, dehydration and side loading (McCarty and Reynolds, 1995). Diffraction data were collected in a N_2 atmosphere using the same instrument and settings as the oriented aggregates, but with longer count times of 17 s per 0.02 degree increment, from 5 to 65º2θ.

Determination of the weight concentration of the interstratified layers in a mixed-layer phase

Simulation of the experimental XRD patterns allows us to determine, first, the quantity of each phase in a sample and second, relative amounts of layer types interstratified in each mixed-layer phase present. To determine the quantity or weighted concentration of each layer type in each mixed-layer phase, the following procedure is used. Let us assume that the weight

https://doi.org/10.1346/CCMN.2004.0520503 Published online by Cambridge University Press

concentration of a mixed-layer structure in which A and B layers are interstratified is equal to m% of total sample. If the contents of A and B layers are equal to W_A and W_B, respectively, and their lateral dimensions are the same, then the ratio of weight concentrations of A and B layers, C_A and C_B, is equal to

$$C_A/C_B = W_A M_A / W_B M_B \quad (1)$$

where M_A and M_B are the molecular weights of A and B layer unit-cells, respectively.

Because $C_A + C_B = m$ one can determine C_A and C_B if M_A and M_B are known. It is assumed that the values of m, W_A and W_B are determined by simulation of the experimental XRD pattern of a sample under study. The C_A and C_B values may be used to determine cation composition of the layer types if the total chemical composition of a sample under study is known (see below).

FTIR analysis and sample preparation of clays

As with the clay separation for XRD, bulk samples for FTIR analysis were treated using the buffered Na acetate and Na dithionite methods of Jackson (1985). The <2.0 μm size fraction was obtained by centrifugation and drying in an oven at ~80ºC. Approximately 100 mg of this dried sample was suspended in 150 mL of distilled water using an ultrasonic probe and freeze dried (McCarty and Reynolds, 1995).

Potassium bromide pellets for transmission FTIR were prepared as follows: (1) 5 mg of sample were combined with 95 mg of pre-packaged KBr (first mixture) and mixed in a Retsch® MM200 mill for 15 min. (2) 40 mg of material from the first mixture were combined with 460 mg of pre-packaged KBr (second mixture) and mixed for 15 min. (3) 200 mg of material from the second mixture were placed in a 13 mm vacuum pellet die and pumped to a pressure of ~9072 kg on the die for 10 min. (4) The finished pellet was then placed in a vacuum oven at 185ºC, and a vacuum of 762 mm of Hg was applied for a minimum of 14 h. (5) A single beam pattern was obtained from the pellet. (6) The pellet was then removed from the beam path with a magnet without exposing the test chamber to the atmosphere and a blank background was obtained. (7) Background correction and IR absorbance conversion were made automatically with the Nicolet® Omnic Software Version 5.0

Elemental analysis

Major element inductively coupled plasma-atomic emission spectroscopy (ICP-AES) was done by XRAL Laboratories, Toronto Canada, on aliquots of the seven <2 μm clay separations chosen for detailed study.

Mössbauer spectroscopy

Mössbauer spectra were obtained using a constant acceleration spectrometer and a source of ^{57}Co in Pd. Isomer shifts are given relative to the centroid of the spectrum of the α-Fe at room temperature. The analysis was performed on Na-saturated <2 μm clay separations at room temperature and with absorbed plane at an angle of 54.7º to the radiation. Lorentzian line shape was used to determine ferrous and ferric octahedral cations ratios.

Scanning electron microscopy

A Phillips E-3 environmental scanning electron microscope (ESEM) equipped with a thin window (light element) Thermo Noran energy-dispersive spectrometer (EDS) was used to obtain magnified images of the samples under study. Samples used in the ESEM do not require cleaning or coating with conductive material prior to imaging. This enables the sample to be analyzed in its natural state.

RESULTS

The complete whole-rock mineralogy summary of all the samples studied in the Isle of Wight section from which the clay separations were taken is shown in Table 1. One can see that the major contributors to the non-clay phase composition are quartz, feldspars and/or calcite whereas among clay minerals 'dioctahedral' Al-rich or Fe-rich 2:1 phases prevail.

After inspection of the routine diffraction data from the <2 μm size fraction of the collected samples, seven were chosen for detailed structural analysis by computer simulation and compositional analysis by ICP. These samples were judged to cover the whole range of the main diffraction features observed for the sample collection. The Lower Cretaceous stratigraphy along with the position of the seven samples studied in detail is shown in Figure 2. The ICP elemental analysis of <2 μm aliquots of the seven samples is shown in Table 2 along with the $Fe^{2+}/(Fe^{2+}+Fe^{3+})$ ratios determined from the Mössbauer spectra decomposition.

Determination of layer types present

Inspection of the diffraction data indicated that two 1:1 layer clays, kaolinite and a serpentine mineral, were present in some samples. Before beginning the computer simulation work, acid susceptibility and FTIR spectroscopy were used to determine the layer types present in each sample. Figure 3a–b compares the diffraction data from samples 10-HL 7 and 16-HL 24 before and after treatment in 1 N HCl. In sample 10-HL 7, essentially all of the ~7 Å phase dissolved as did the 15 Å phase indicating that the main clay minerals in the sample are Fe-rich. The only clay that remained after this treatment was mica and chlorite, presumably Mg-rich. As in sample 10-HL 7, all minerals except 10 Å illite were dissolved after the treatment of sample 16-HL 24. These data indicate that the 7 Å phase is a serpentine mineral that we suspected to be berthierine.

https://doi.org/10.1346/CCMN.2004.0520503 Published online by Cambridge University Press

Table 1. Whole-rock mineralogy from quantitative X-ray phase analysis.

Sample	ID	Qtz	Kspar	Plag	Cal	Mg-Cal	Dol	Py	Sid	Gyp	Anat	Hem	Zeol	Amph	Sum non-clay	Kaol	2:1 Al clay	2:1 Fe clay	Chl	Tri 1:1	Sum clay	Total
8	BG 16	18	0.9	1	12	0.3	0	2	0.4	0	0	0	0	0	34	0	9	56	0.4	0.2	65	99
*7	BG 15	16	0	1	19	2	0	0.9	0.9	0	0	1	0	0	41	0	0	59	0	0	59	100
6	BG 11	29	5	13	0	0	0	0	0	0	0	0	0	0	46	3	41	2	6	1	53	99
*5	BG 07	29	4	13	0.1	0.9	0	0.1	0.2	0	0.8	0	0	0	48	5	36	5	4	0	50	97
4	BG 03	22	5	13	0	0	0	0	0.3	0	0.5	0	0	0	40	5	37	9	6	0.5	57	97
3	BG 01	17	2	7	0.2	2	0	0	1	0	0.5	0	0	0	28	6	45	11	4	2	67	95
18	HL 29	25	2	14	0	0	2	0.6	0.5	0	0.4	0	0	1	45	4	21	14	7	6	51	96
17	HL 25	25	2	14	0	0.4	1	0.3	0.2	0	0	0	0	3	46	2	15	19	6	9	51	98
*16	HL 24	51	2	16	0	0	0	0	0.4	0	0	0	0	2	72	0	6	11	5	5	27	99
15	HL 22	20	3	9	0	1	0	0	0.1	0	0.5	0	0	0	34	6	45	5	4	3	62	96
*14	HL 18	88	0	0	0	0	0	0	0	0	0	0	0	0	88	0	1	11	0	0	12	100
13	HL 15	32	2	17	0	1	2	0.4	0.5	0	0.6	0.5	0	3	59	5	17	7	9	3	39	98
12	HL 13	88	0	0	0	0	0	0	0	0	0	0	0	0	88	0	2	10	0	0.1	12	100
11	HL 10	25	2	10	0	0	0	0.3	0	0	0	0	0	0.7	37	1	10	34	5	13	63	100
*10	HL 07	26	3	12	0	0	0	0	0	0	0	0.2	0	1	42	2	17	19	9	12	58	100
9	HL 03	27	2	12	0	0.2	0	0.1	0.2	0	0	0	0	2	43	4	16	17	5	13	54	98
31	WC 15	29	2	18	0	0	1	0.3	0.6	0	0.5	0	0	1	53	3	18	10	9	3	43	96
30	WC 13/14	5	0	0	7	0	0	8	0	0.4	0	0	0	0	20	0	0	80	0	0	80	100
29	WC 10	29	2	17	0	0.1	2	0.6	0.6	0.7	0.8	0	0	1	53	5	20	6	9	2	42	95
28	WC 07	5	0	0	22	0	0	3	0.8	0.3	0	0	0	0	31	0	1	66	0	1	67	99
27	WC 03	25	3	15	0	0	2	0.3	0.5	0.4	0	0.1	0	0.8	46	5	22	10	8	4	49	95
*26	WC 01	27	2	15	0	0.3	2	0.1	0.4	0.1	0.4	0.5	1	1	50	5	24	8	9	4	49	100
25	LGB 18	30	3	13	0.1	0.7	1	0.5	0.6	0.5	1	0.8	0	1	53	4	18	16	8	1	46	99
24	LGB 17	17	2	8	0.7	0	0.6	0.1	0.1	0.5	0.4	0.3	0.7	0.1	31	5	48	8	4	3	67	97
23	LGB 13/14	4	0	1	33	0.9	0	0.5	2	0	0	1	0	0.7	43	0	3	46	0	1	51	94
22	LGB 10	24	1	14	0	0	2	0.5	0.6	0	0.7	0.5	0	1	44	7	24	11	7	4	53	96
*21	LGB 07	22	2	11	0	0	0.3	0	0	2	0.7	0	0	0.7	38	3	40	14	2	3	61	100
20	LGB 04	7	0	1	19	1	0	0.7	1.5	0	0	1	3	0.2	34	0	1	61	1	2	65	100
19	LGB 03	39	3	14	0	0	1	0.4	0.5	0	0.2	0	0	1	59	4	19	7	6	5	41	100
2	BH 2	28	0	12	6	0	0	0.2	0.5	0	0.1	0	0	0	47	1	48	4	0	0.9	53	100
1	BH 1	6	0	2	51	7	0	0.2	0.7	0	0	0	0	0	66	2	3	25	0	0	30	96

Qtz = quartz; Plag = plagioclase feldspar; Kspar = K-feldspar; Cal = calcite; Mg-cal = Mg-calcite; Dol = dolomite; Py = pyrite; Sid = siderite; Gyp = gypsum; Anat = anatase; Hem = hematite; Zeol = zeolite; Amph = amphibole; Kaol = kaolinite; 2:1 Al clay = illite, illite-smectite, smectite, and possibly, muscovite; 2:1 Fe clay = Fe-rich illite, glauconite-nontronite, and nontronite; Chl = chlorite; Tri 1:1 = trioctahedral 1:1 layer clays. * = samples chosen for detailed study.

Table 2. Elemental oxides determined by chemical analysis and Mössbauer spectroscopy (1) and by calculations using the average weighted concentrations and structural formulae of the layers comprising the separations (2).

Sample	SiO_2	Al_2O_3	Fe_2O_3	FeO	MgO	K_2O	CaO	$Fe^{2+}/(Fe^{3+}+Fe^{2+})_{total}$
21-LGB 7(1)	53.25	21.32	4.98	1.68	2.48	2.49	1.66	0.2
21-LGB 7(2)	53.23	21.29	5.00	1.72	2.48	2.49	1.72	
5-BG 7(1)	51.62	23.78	4.02	2.80	2.69	2.52	1.55	0.34
5-BG 7(2)	51.24	23.78	4.14	2.85	2.80	2.65	1.17	
10-HL 7(1)	39.42	13.11	17.52	11.20	3.32	2.90	1.39	0.39
10-HL 7(2)*	39.60	13.19	17.60	11.70	3.38	2.80	1.20	
16-HL 24(1)	37.44	13.64	15.49	14.52	5.15	1.79	2.00	0.51
16-HL 24(2)	37.43	13.65	13.50	14.55	5.13	1.56	1.01	
26-WC 1(1)	43.07	19.11	8.17	7.62	6.08	1.52	1.90	0.41
26-WC 1(2)	43.10	19.11	8.19	7.67	6.05	1.52	1.24	
7-BG 15	54.35	9.80	16.88	1.38	4.02	6.28	2.80	0.08
14-HL 18	52.30	15.00	14.06	1.74	2.53	8.01	0.59	0.12

% Chemical analyses are from the <2 μm size fraction
* 3% of K-feldspar was added to the 10-HL 7 phase composition
Total Fe as Fe_2O_3

In contrast to the behavior of the clays in these two samples, when sample 26-WC 1 was treated with HCl, the 14.98 Å phase dissolved but the 7 Å phase in this sample is kaolinite because the treatment did not significantly change the basal reflections at 7.15 Å and 3.57 Å (Figure 3c). However, the intensities of the reflections at 7.10 Å and 3.54 Å significantly decreased after the treatments probably because of the coexistence of kaolinite with berthierine or Fe-rich chlorite. Similar modification of basal reflections at ~ 7 Å and 3.5 Å is observed for sample 5B-G 7 treated with HCl (Figure 3d). However, in this case the decrease in the basal reflections intensities at 7.10 Å and 3.54 Å may be associated with the presence of a significant amount of Fe-rich chlorite, the basal reflections of which are clearly observed in the untreated XRD patterns.

Figure 4 shows the OH-stretching vibration region of the IR spectra of the samples under study. Samples 5-BG 7 and 21-LGB 7 have similar spectra that contain sharp intensive maxima at ~3620 and 3700 cm^{-1}, which indicates the presence of kaolinite layers (Farmer, 1974). The broad band between these two peaks should refer to Al-OH-Al stretching vibrations in the 2:1 layers. A distinct shoulder at 3605 cm^{-1} in the spectra corresponds to Al-OH-Mg vibrations.

The spectrum of 7-BG 15 shows a complex absorption band with distinct peaks at 3538, 3566 and 3600 cm^{-1}. According to Besson and Drits (1997), the bands should refer to Fe^{3+}-OH-Fe^{3+}, Mg-OH-Fe^{3+} and Al-OH-Mg vibrations, respectively, in mica-like layers. The spectrum of 14-HL 18 shows two distinct regions, one with sharp strong maxima at 3534 and 3560 cm^{-1} and another with pronounced peaks at 3602 and 3621 cm^{-1}. These bands refer to Fe^{3+}-OH-Fe^{3+}, Mg-OH-Fe^{3+}, Al-OH-Mg and Al-OH-Al vibrations in the mica-like layers (Besson and Drits, 1997).

The spectra of samples 10-HL 7 and 16-HL 24 both show a very broad absorption band around 3550 cm^{-1} that could be the superposition of several cation-OH-cation stretching vibrations which involve Fe. The shape and the position of the band may indicate the presence of Fe-rich 2:1 layers. In addition, both spectra show a broad band around 3400−3440 cm^{-1} that could refer to additional phases, *e.g.* trioctahedral chlorite and/or trioctahedral 1:1 phyllosilicates, such as berthierine, which, according to Farmer (1974), show broad bands in this region (chlorite, at 3417−3437 cm^{-1} and berthierine, at 3420 cm^{-1}). The second characteristic band present in the spectra of these minerals (3535−3575 and 3560 cm^{-1} for chlorite and berthierine, respectively) would be masked by the cation-OH-Fe stretching vibrations in the 2:1 layers. This interpretation of the IR spectra is in agreement with the acid treatment of samples 10-HL 7 and 16-HL 24 accompanied by the dissolution of the 7 Å phase.

The spectrum of sample 26-LGB 7 shows features characteristic of the spectra of samples 5-BG 7 and 21-LGB 7 as well as of samples 10-HL 7 and 16-HL 24. It means that this sample, along with kaolinite and Al-rich 2:1 layers, contains berthierine and/or chlorite and Fe-rich 2:1 layers.

Thus, the XRD patterns after acid treatment, and the interpretation of the IR spectra of the original samples show that samples 5-BG 7 and 21-LGB 7 consist of kaolinite, illite, chlorite and Fe-bearing 2:1 layers, whereas samples 10-HL 7 and 16-HL 24 contain berthierine, illite and Fe-rich 2:1 layers. Sample 26-LGB 7, along with kaolinite, may contain berthierine layers as well as Fe-rich 2:1 layers.

Simulation of the experimental XRD patterns

The XRD patterns of samples 14-HL 18 and 7-BG 15 are similar and contain rational series of basal reflections with the period along the *c* axis equal to 10 Å. The low intensity of the 002 reflection indicates that the 10 Å mineral belongs to glauconite (Figure 5). Both samples were found to consist of a mixed-layer phase in

https://doi.org/10.1346/CCMN.2004.0520503 Published online by Cambridge University Press

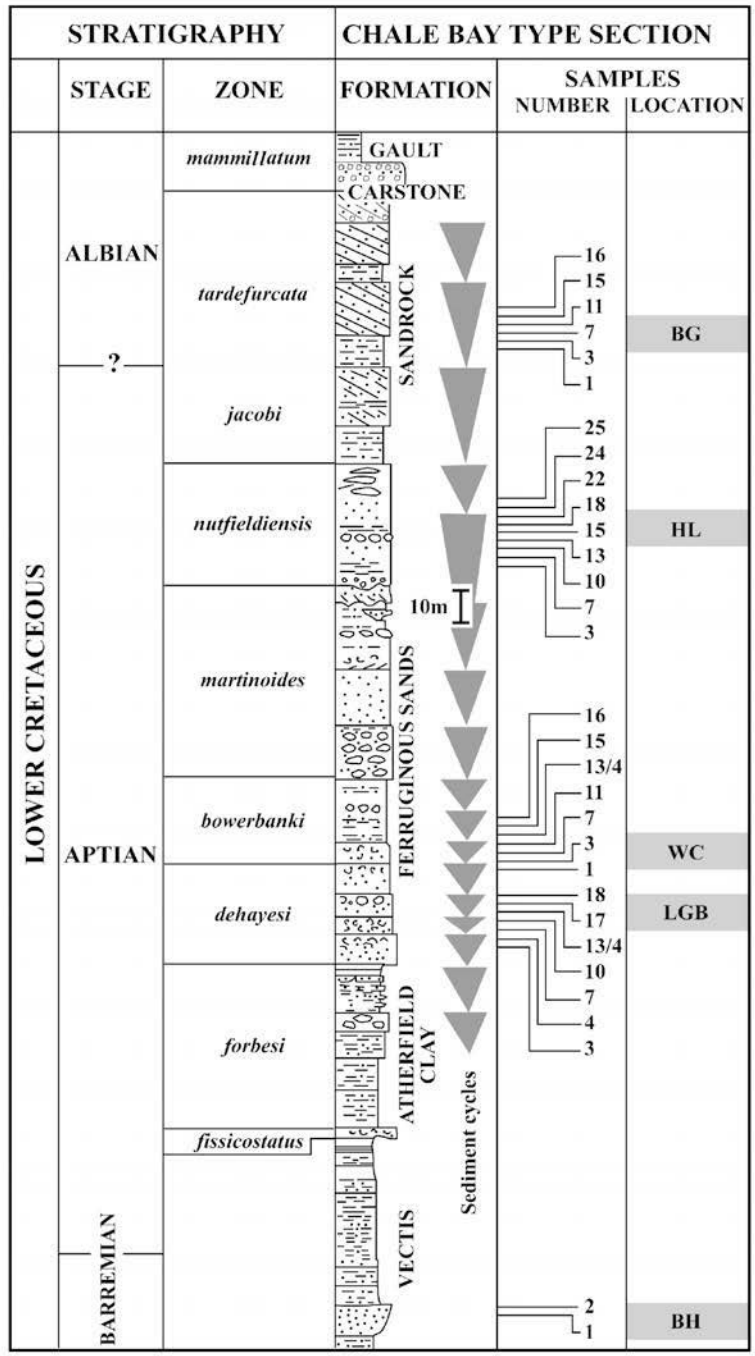

Figure 2. Stratigraphic column with sample locations of detailed clay samples. BG = Blackgang samples. HL = Horse Ledge samples. WC = Whale Chine samples. LGB = Lower Gryphea Bed samples.

which 91–92% of glauconite and 8–9% of expandable layers are interstratified. The expandable layers are represented by nontronite and vermiculite. In contrast to the single phase in sample 14-HL 18, sample 7-BG 15 is a physical mixture of GL-NR-V with a small amount of discrete nontronite (Figure 5, Table 3).

Sample 5-BG7 along with discrete illite (24%), kaolinite (7%) and chlorite (8%) contains two mixed-layer phases: I-S (26%) and kaolinite-smectite-vermiculite (K-S-V) (35%) (Figure 6a–b). The I-S consists of 60% illite and 40% smectite layers that are interstratified with some tendency to segregation ($P_{SS} > W_S$, Table 3). The degree of this segregation can be estimated by the following equation:

$$S_1 = (P_{SS} - W_S)/(1 - W_S) \quad (2)$$

https://doi.org/10.1346/CCMN.2004.0520503 Published online by Cambridge University Press

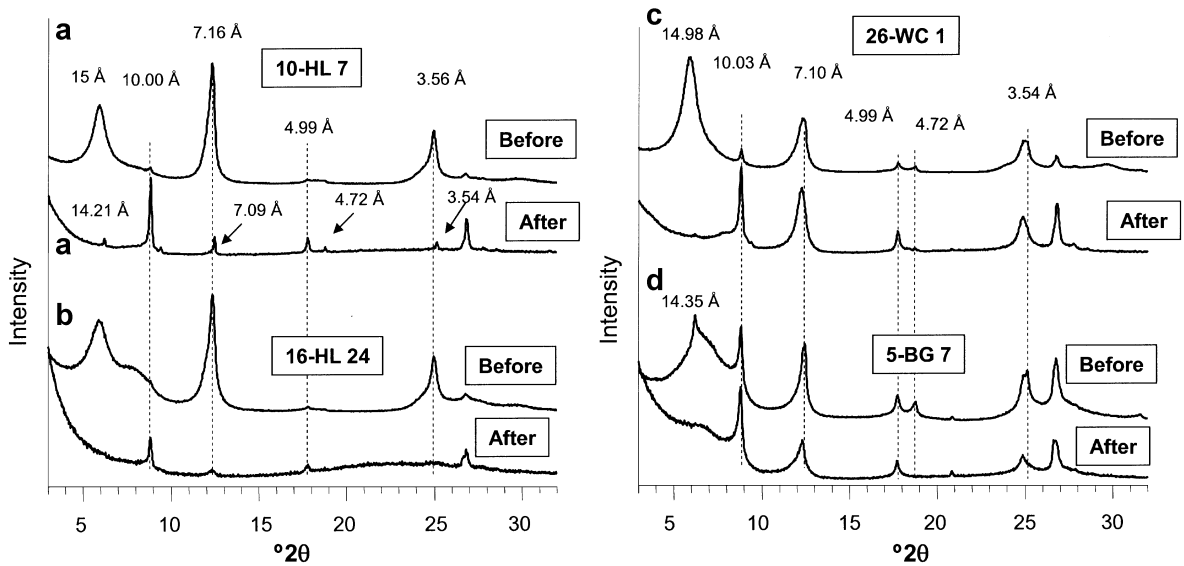

Figure 3. Diffraction data from the <2 μm, air-dried and acid-treated (1 N HCl) samples: (a) 10-HL 7, (b) 16-HL 24, (c) 26-WC 1 and (d) 5-BG 7, showing the relative solubility of layer types.

where $S_1 = 0$ when $W_S = P_{SS}$ and R = 0 and $S_1 = 1$ when $P_{SS} = 1$ in the case of complete segregation. For I-S, $S_1 = 0.33$. In the K-S-V, the layer types are interstratified in proportions 0.75:0.13:0.12 at R = 0 (Table 3).

Despite the fact that the experimental XRD patterns of samples 5-BG 7 and 21-LGB 7 look very different (Figures 6a–b and 7a–b) their phase compositions are similar. In both samples, the major components are represented by I-S and K-S-V, each of which contains almost identical amounts of the interstratified layer types and similar patterns in their alternation (Table 3). The main difference in the compared phase composition is that sample 21-LGB 7 contains discrete smectite (11%, Table 3) and its presence dramatically changes the XRD pattern in comparison with that of sample 5-BG 7.

Simulation of the XRD patterns of sample 10-HL 7 reveals an unusual assemblage of Fe-rich mixed-layered GL-NR-V (25%), Br-NR-V (35%), NR-V-Br (12%) and discrete berthierine (23%) and illite (4%) (Figure 8a–b, Table 3). The main difference between the Br-NR-V (0.75: 0.20: 0.05) and NR-V-Br (0.65: 0.10: 0.25) is that berthierine layers prevail in the first phase and expandable layers, in the second.

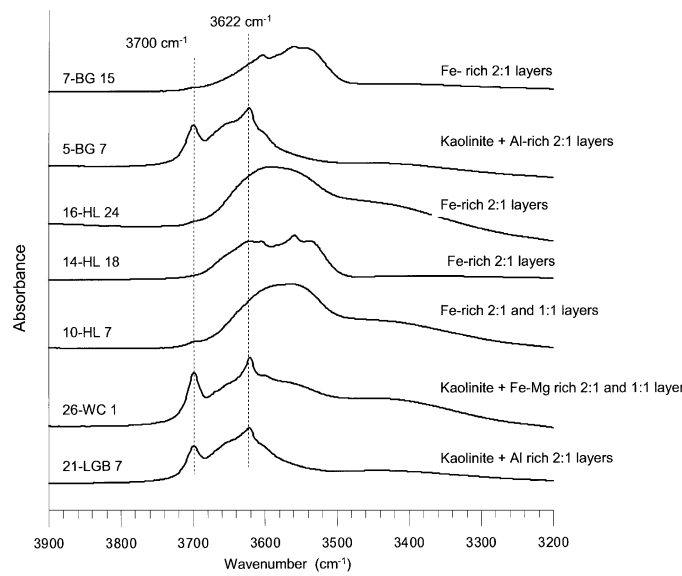

Figure 4. FTIR spectra from OH-stretching region that shows three samples which contain high kaolinite (strong absorbance frequencies at 3700 and 3622 cm^{-1}) and other frequencies diagnostic of Al- and Fe-rich 2:1 and Fe-rich 1:1 layers.

https://doi.org/10.1346/CCMN.2004.0520503 Published online by Cambridge University Press

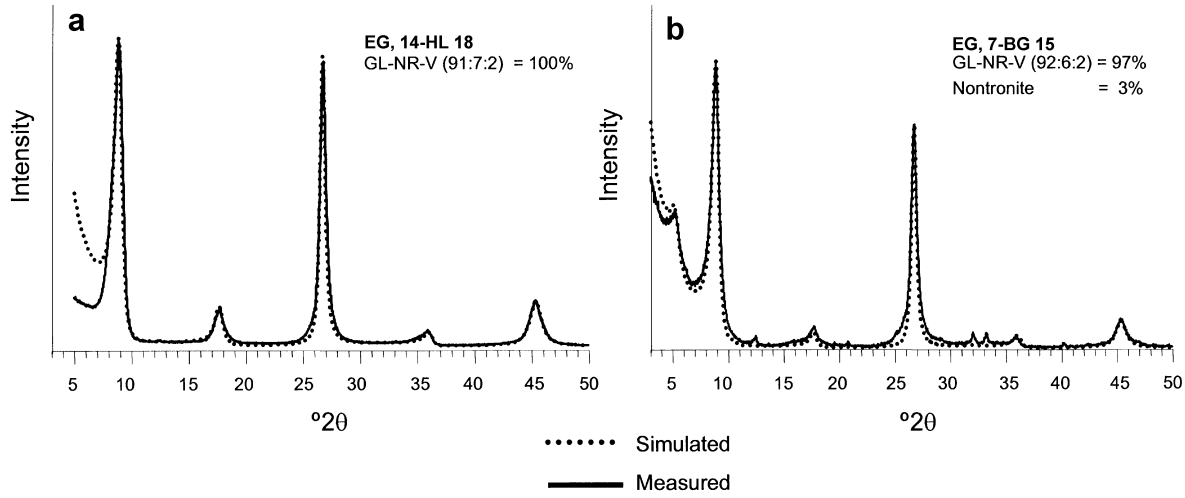

Figure 5. Diffraction data and computer simulation for <2 μm oriented preparation for sample (a) 14-HL 18 and (b) 7-BG 15.

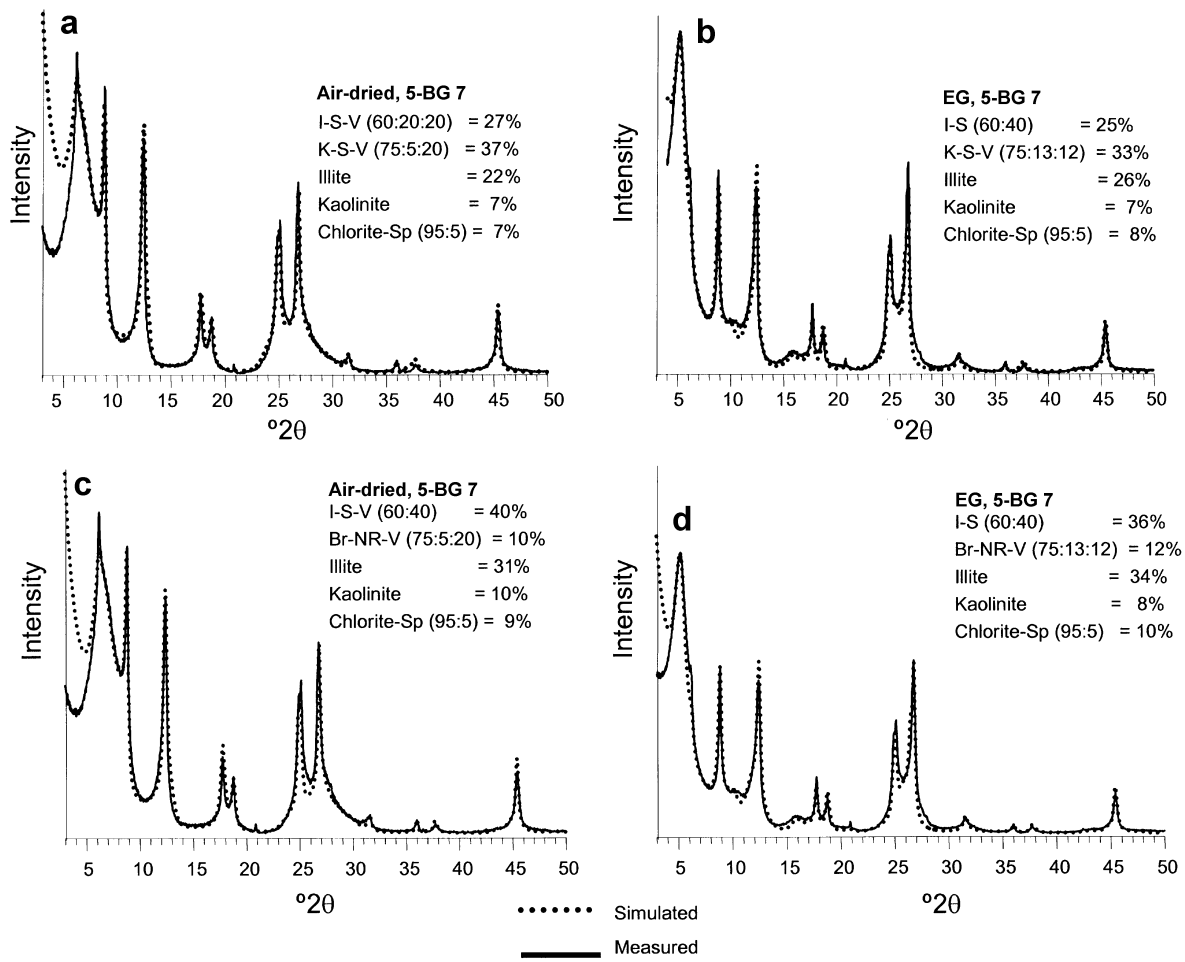

Figure 6. Diffraction data and computer simulations for <2 μm oriented preparation for sample 5-BG 7 (a,b), showing the simulation with kaolinite as the 7 Å layer in a mixed-layer structure compared with a simulation for the same sample with berthierine as the 7 Å layer in the mixed-layer structure while all other parameters are constant (c,d); note the difference in phase content (see text).

https://doi.org/10.1346/CCMN.2004.0520503 Published online by Cambridge University Press

Table 3. Weighted concentrations (%) of coexisting discrete and mixed-layer phases as well as layer types, their thickness (Å) and content determined by XRD simulation are given for specimens of each studied sample in air-dried and ethylene glycol-solvated states.

EG, 7-BG 15	Air-dried, 5-BG 7	EG, 5-BG 7	Air-dried, 16-HL 24	EG, 16-HL 24	EG, 14-HL 18
GL-NR-V = 97% 9.98 - 6.86 - 14.0 0.92 - 0.06 - 0.02	I-S-V = 27% 9.98 - 14.8 - 12.5 0.60 - 0.20 - 0.20 *P*(ss) = 0.4, *P*(sv) = 0.2	I-S = 25% 9.98 - 16.95 0.60 - 0.40 *P*(ss)=0.6	Br-Ch-S = 50% 7.0 - 14.0 - 15.0 0.50 - 0.20 - 0.30	Br-Ch-S = 42% 7.0 - 14.0 - 16.6 0.50 - 0.20 - 0.30	GL-NR-V = 100% 9.98 - 16.86 - 14.0 0.91 - 0.07 - 0.02
NR = 3% 16.76	P(vs)=0.2, *P*(vv)=0.4		NR-Br-V = 9% 14.8 - 7.0 - 12.5 0.60 - 0.20 - 0.20	NR-Br-V = 13% 16.7 - 7.0 - 12.9 0.50 - 0.20 - 0.30	
	K-S-V = 37% 7.16 - 15.5 - 12.5 0.75 - 0.05 - 0.20	K-S-V = 33% 7.16 - 16.9 - 12.9 0.75 - 0.13 - 0.12	GL-NR-V = 7% 9.98 - 14.9 - 12.3 0.70 - 0.20 - 0.10	GL-NR = 7% 9.98 - 16.6 0.70 - 0.30	
	Illite = 22% 9.98 - 12.5 0.98 - 0.02	Illite = 26% 9.98 - 12.5 0.98 - 0.02	Berthierine-like = 22% 7.13	Berthierine-like = 27% 7.13	
	Kaolinite = 7% 7.16	Kaolinite = 7% 7.16	Illite = 10% 9.98	Illite = 9% 9.98	
	Chlorite-Sp = 7% 14.18 - 7.09 0.95 - 0.05	Chlorite-Sp = 8% 14.18 - 7.09 0.95 - 0.05	Chlorite-Sp = 2% 14.18 - 7.09 0.95 - 0.05	Chlorite-Sp = 2% 14.18 - 7.09 0.95 - 0.05	

Air-dried, 10-HL 7	EG, 10-HL 7	Air-dried, 26-WC 1	EG, 26-WC 1	Air-dried, 21-LGB 7	EG, 21-LGB 7
GL-NR-V = 27% 9.98 - 14.9 - 12.3 0.70 - 0.20 - 0.10	GL-NR-V = 23% 9.98 - 16.75 - 12.9 0.70 - 0.20 - 0.10	NR-Br-V = 25% 14.9 - 7.10 - 12.5 0.70 - 0.20 - 0.10	NR-Br-V = 30% 16.6 - 7.10 - 12.9 0.70 - 0.20 - 0.10	I-S-V = 37% 9.98 - 12.5 - 15.1 0.60 - 0.25 - 0.15 *P*(ss) = 0.34, *P*(sv) = 0.21	I-S = 34% 9.98 - 16.85 0.60 - 0.40 *P*(ss) = 0.55
Br-NR-V = 33% 7.13 - 14.8 - 12.5 0.75 - 0.15 - 0.10	Br-NR-V = 37% 7.13 - 16.6 - 12.9 0.75 - 0.20 - 0.05	Br-NR-V = 25% 7.10 - 15.15 - 12.5 0.70 - 0.20 - 0.10	Br-NR-V = 25% 7.10 - 16.6 - 12.9 0.70 - 0.20 - 0.10	*P*(vs) = 0.34, *P*(vv) = 0.21 K-S-V = 34% 7.16 - 15.5 - 12.5 0.70 - 0.12 - 0.18	K-S-V = 31% 7.16 - 16.85 - 12.9 0.70 - 0.15 - 0.15
NR-Br-V = 13% 14.8 - 7.13 - 12.9 0.65 - 0.25 - 0.10	NR-Br-V = 12% 16.6 - 7.13 - 12.9 0.65 - 0.25 - 0.10	Illite = 17% 9.98	Illite = 12% 9.98	Smectite = 9% 15.1 - 12.5 0.70 - 0.30	Smectite = 13% 16.85
Berthierine-like = 23% 7.13	Berthierine-like = 23% 7.13	Kaolinite = 25% 7.15	Kaolinite = 25% 7.15		
Illite = 3% 9.98	Illite = 5% 9.98	Chlorite-Sp = 8% 14.18 - 7.09 0.95 - 0.05	Chlorite-Sp = 8% 14.2 - 7.10 0.95 - 0.05	Kaolinite-S = 4% 7.16 - 15.1 0.95 - 0.05	Kaolinite-S = 5% 7.16 - 16.85 0.95 - 0.05
				Illite = 13% 9.98 - 15.1 - 12.5 0.90 - 0.05 - 0.05	Illite = 15% 9.98 - 17.0 - 14.0 0.90 - 0.05 - 0.05
				Chlorite-Sp = 2% 14.18−7.10 0.95−0.05	Chlorite-Sp = 2% 14.18−7.10 0.95−0.05

GL = glauconite, NR = nontronite, Br = berthierine-like, V = vermiculite, Sp = serpentine, K = kaolinite, I = illite, S = smectite

The clay fraction of sample 16-HL 24 has an even more complex and peculiar phase composition than that of sample 10-HL 7 (Figure 8c−d, Table 3). The dominant phase in this sample (46%) is a three-component structure in which 50% berthierine, 20% chlorite and 30% nontronite layers are interstratified at random. Two other mixed-layer phases have the same (GL-NR) or similar (NR-V-Br) amounts of the layer types as those in analogous phases in sample 10-HL 7 (Table 3).

The <2 μm fraction from sample 26-WC 1 contains two randomly interstratified Br-NR-V and NR-V-Br phases of nearly equal proportions and discrete illite (14%), kaolinite (25%) and trioctahedral chlorite (8%) (Figure 7c). The NR-V-Br is dominated by nontronite

https://doi.org/10.1346/CCMN.2004.0520503 Published online by Cambridge University Press

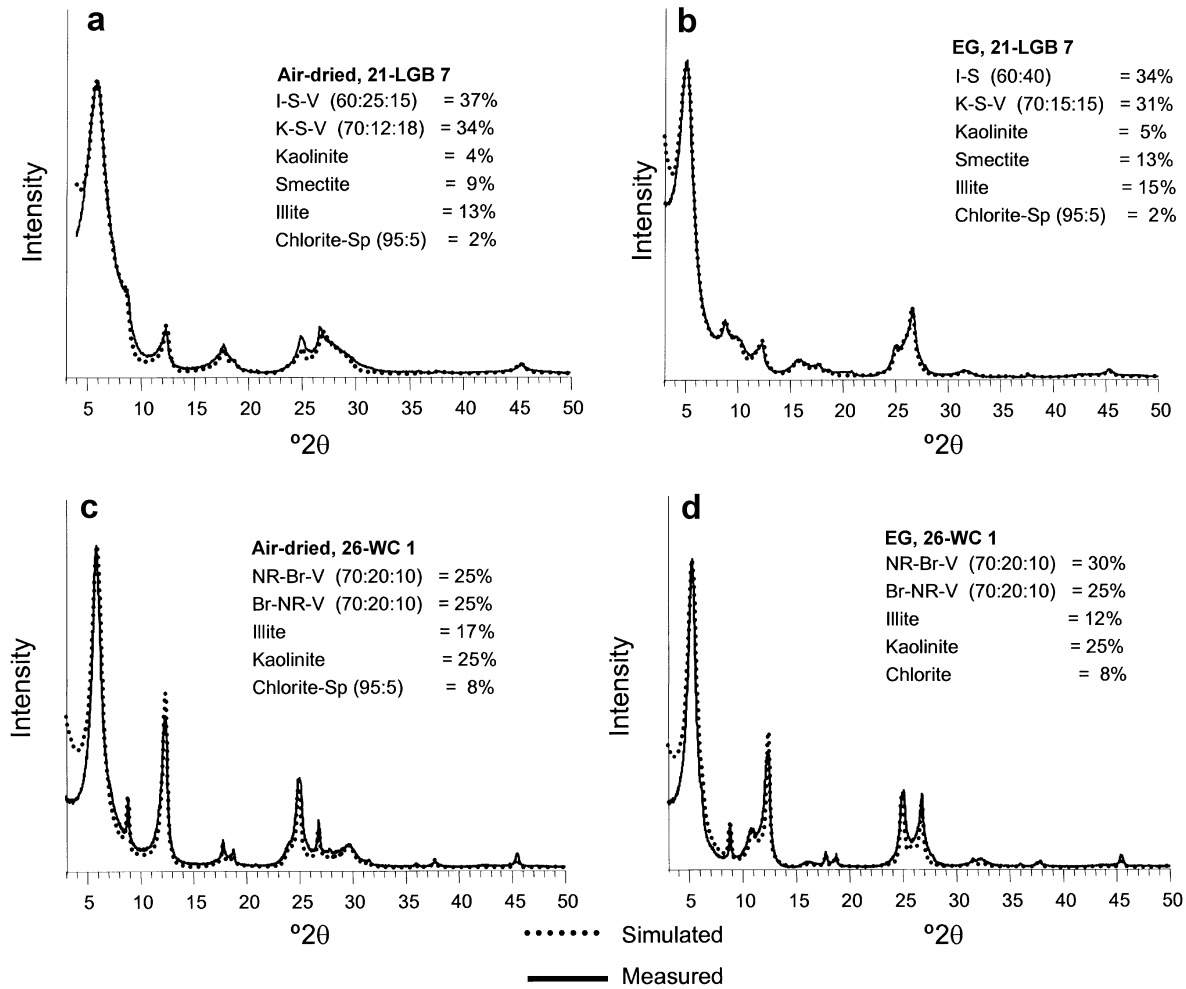

Figure 7. Diffraction data and computer simulations for <2 μm oriented preparation for sample 21-LGB 7 (a,b) and 26-WC 1 (c,d).

layers (70%) with 20% of the berthierine-like layers. In the Br-NR-V, the proportions of these layers are reversed. Both phases have 10% vermiculite layer content. Thus, the phase composition of sample 26-WC 1 is intermediate between those of 5-BG 7 and 10-HL 7. The significant amount of Al-rich illite and kaolinite draws this sample together with 5-BG 7 whereas the presence of the Fe-rich Br-NR-V and NR-Br-V is a feature common with 10-HL 7.

The weight concentrations and averaged structural formulae of the layer types

Table 3 shows quantities of mixed-layer and discrete minerals as well as amounts of the layer types in the mixed-layer phases determined for each sample by XRD simulation. This table shows that certain types of layers are common for discrete and mixed-layer phases. To determine the average cation composition of the coexisting layer types in a sample, one has first to determine the weighted concentrations of the layer types in each mixed-layer phase of the sample.

To illustrate the procedure, the phase composition of sample 21-LGB 7 will be used as an example. For simplicity, cation compositions of expandable layers in the I-S-V and K-S-V found in the sample were assumed to be the same. In addition, using structural formulae typical for kaolinite, illite, $K_{0.75}(Si_{3.5}Al_{0.5})(Al_{1.55}Fe^{3+}_{0.2}Mg_{0.25})O_{10}(OH)_2$, and smectite $Ca_{0.20}(Si_{3.85}Al_{0.15})(Al_{1.55}Fe^{3+}_{0.2}Mg_{0.25})O_{10}(OH)_2 3H_2O$, the molecular weights of the layers equal to 516, 788 and 860, respectively, were calculated. Note that these values have been changed slightly when more realistic formulae for the layers were determined. Table 3 shows that the weighted content of the K-S-V in sample 21-LGB 7 is 33% whereas the amounts of kaolinite and expandable layers are 0.70 and 0.30, respectively. According to equation 1 the ratio of the weighted contents of kaolinite, C_K, and expandable, C_{EXP} layers is:

$$C_K/C_{EXP} = C_K/(33 - C_K) = M_K W_K/M_{EXP} W_{EXP} = (516 \cdot 0.70)/(860 \cdot 0.30) \quad (3)$$

https://doi.org/10.1346/CCMN.2004.0520503 Published online by Cambridge University Press

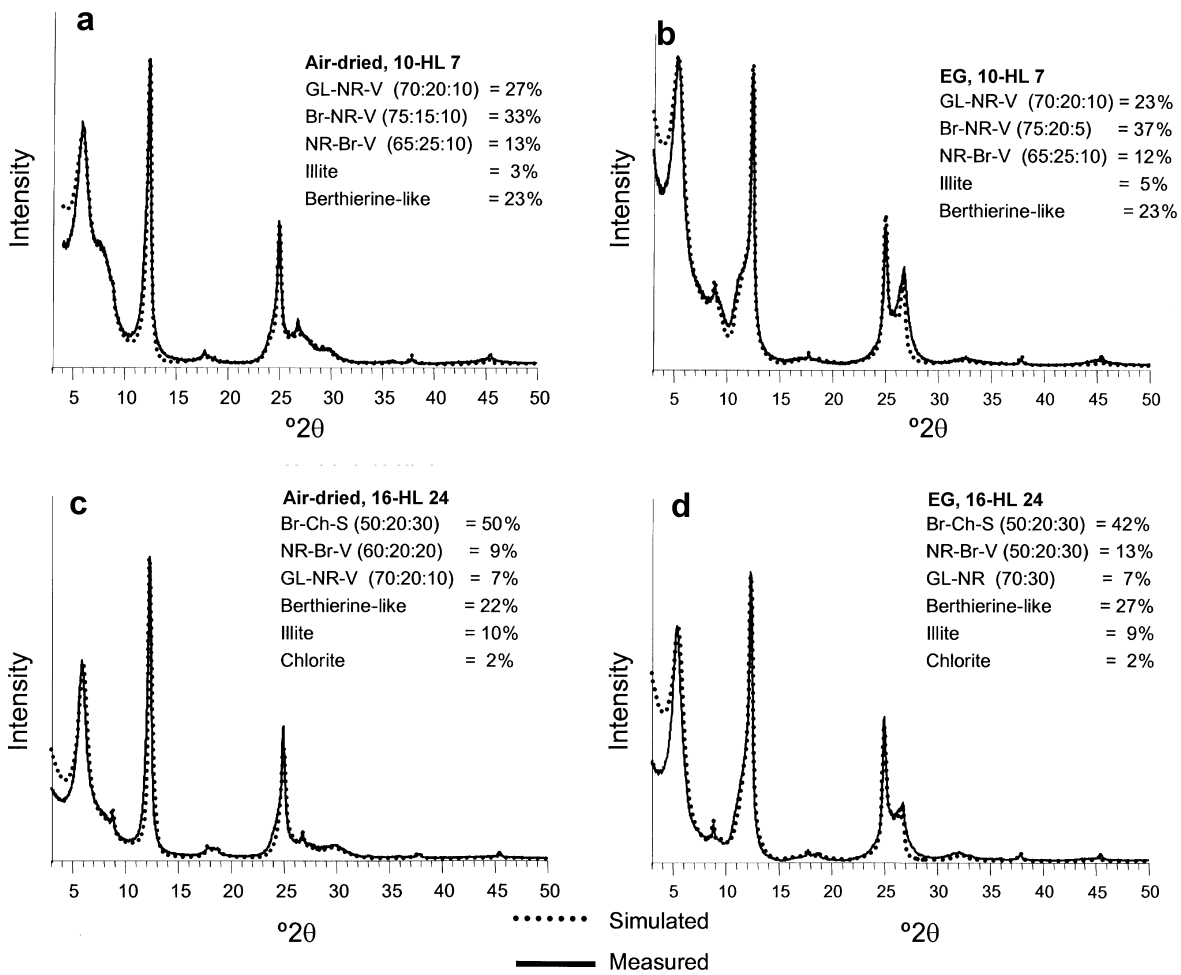

Figure 8. Diffraction data and computer simulations for <2 μm oriented preparation for sample 10-HL 7 (a,b) and 16-HL 24 (c,d).

and thus C_K = 19% and C_{EXP} = 14%. The total content of kaolinite layers in the sample should be equal to the sum of 19% from the K-S-V and 5% from discrete kaolinite.

Similarly, the weighted contents of illite, smectite and trioctahedral chlorite layers in sample 21-LGB 7 were found to be equal to 34, 40 and 2%, respectively. Using the trial-and-error approach the average structural formulae were determined for illite and smectite layers by partitioning the elemental oxide contents into the amount of each layer type. Naturally the calculated formulae differ from the initial 'idealized' ones. For example, for illite layers, amounts of K and Al_{tetr} per $O_{10}(OH)_2$ decrease from 0.75 and 0.50 atoms in the idealized formula to 0.60 and 0.30 atoms in the calculated one (Table 4). In the case of smectite layers the total amount of Fe significantly increases in comparison with that given in the idealized formula (0.60 *vs.* 0.20 atoms per $O_{10}(OH)_2$).

The formulae, however, are reasonable from a crystal-chemical point of view and satisfy the total chemical analysis of the samples (Table 2) when the weight concentrations of illite, smectite, kaolinite and chlorite layers are to 34, 44, 20 and 2%, respectively. This result indicates that the layer concentrations determined by simulation and the approach described are quite similar. The structural formulae for particular layers along with weighted concentrations of layers coexisting in each studied sample are given in Table 4. Table 2 compares the elemental oxides determined experimentally and calculated from the average structural formulae and weight concentrations of the layers composing each sample.

Except for CaO content, a satisfactory agreement between the compared amounts of oxides is observed. Note that the structural formulae for berthierine-like layers correspond to di-trioctahedral varieties because the sum of octahedral cations is significantly less than 6 atoms per unit-cell. The specific feature of the octahedral cation composition of the layers is that the contents of Fe^{3+} and Fe^{2+} are significantly greater than those of Al and Mg^{2+}, respectively. Structural formulae of the almost monomineral GL-NR-V in samples

https://doi.org/10.1346/CCMN.2004.0520503 Published online by Cambridge University Press

Table 4. Structural formulae and weighted concentrations of layer types comprising the <2 μm fractions of the studied samples; the procedure for calculation is described in the text.

Sample	Illite/mica $O10(OH)_2$	Glauconite $O_{10}(OH)_2$	Fe-smectite $O_{10}(OH)_2$	Nontronite $O_{10}(OH)_2 \cdot 3H_2O$	Berthierine-like layer $O_{10}(OH)_8$	Kaolinite	Chlorite $O_{10}(OH)_8$
7-BG 15		100% $K_{0.56}Ca_{0.11}Na_{0.01}(Si_{3.79}Al_{0.21})$ $(Al_{0.59}Fe^{3+}_{0.88}Fe^{2+}_{0.08}Mg_{0.42})$					
5-BG 7	37% $K_{0.60}(Si_{3.75}Al_{0.25})$ $(Al_{1.35}Fe^{3+}_{0.3}Fe^{2+}_{0.1}Mg_{0.25})$		30% $Ca_{0.15}Si_{4.00}$ $(Al_{1.35}Fe^{3+}_{0.35}Fe^{2+}_{0.20}Mg_{0.10})$			25% $Si_4Al_4O_{10}(OH)_8$	8% $(Si_{3.20}Al_{0.80})$ $(Al_{1.76}Fe^{3+}_{0.22}Fe^{2+}_{2.02}Mg_{1.38})$
26-WC 1	16% $K_{0.8}(Si_{3.4}Al_{0.6})$ $(Al_{1.6}Fe^{3+}_{0.2}Mg_{0.2})$			33% $Ca_{0.34}(Si_{3.92}Al_{0.08})$ $(Al_{0.44}Fe^{3+}_{0.96}Fe^{2+}_{0.35}Mg_{0.25})$	22% $(Si_{3.28}Al_{0.72})$ $(Al_{0.82}Fe^{3+}_{0.81}Fe^{2+}_{2.15}Mg_{1.77})_{5.55}$	20% $Si_4Al_4O_{10}(OH)_8$	9% $(Si_{2.66}Al_{1.34})$ $(Al_{1.34}Fe^{2+}_{0.5}Mg_{4.16})$
16-HL 24	10% $K_{0.90}(Si_{3.25}Al_{0.75})$ $(Al_{1.75}Fe^{3+}_{0.10}Mg_{0.15})$	5% $K_{0.9}(Si_{3.42}Al_{0.58})$ $(Al_{0.65}Fe^{3+}_{1.03}Mg_{0.32})$		26% $Ca_{0.35}(Si_{3.65}Al_{0.35})$ $(Al_{0.45}Fe^{3+}_{1.2}Mg_{0.35})$	59% Ch+Br $(Si_{3.25}Al_{0.75})$ $(Al_{0.85}Fe^{3+}_{1.19}Fe^{2+}_{2.22}\ Mg_{1.11})_{5.37}$		
14-HL 18		100% $K_{0.71}Ca_{0.04}(Si_{3.65}Al_{0.35})$ $(Al_{0.88}Fe^{3+}_{0.73}Fe^{2+}_{0.10}Mg_{0.26})$					
10-HL 7*	6% $K_{0.90}(Si_{3.30}Al_{0.70})$ $(Al_{1.70}Fe^{3+}_{0.1}Mg_{0.2})$	16% $K_{0.90}(Si_{3.40}Al_{0.60})$ $(Al_{0.65}Fe^{3+}_{1.05}Fe^{2+}_{0.05}Mg_{0.25})$		27% $Ca_{0.35}(Si_{3.7}Al_{0.3})$ $(Al_{0.75}Fe^{3+}_{0.85}Fe^{2+}_{0.15}Mg_{0.25})$	48% $(Si_{3.15}Al_{0.85})$ $(Al_{0.56}Fe^{3+}_{1.79}Fe^{2+}_{2.12}Mg_{0.79})_{5.26}$		
21-LGB 7	34% $K_{0.60}(Si_{3.70}Al_{0.30})$ $(Al_{1.5}Fe^{3+}_{0.20}Mg_{0.30})$		44% $Ca_{0.32}(Si_{3.94}Al_{0.06})$ $(Al_{1.0}Fe^{3+}_{0.43}Fe^{2+}_{0.23}Mg_{0.34})$			20% $Si_4Al_4O_{10}(OH)_8$	2% $(Si_{3.30}Al_{0.70})$ $(Fe^{3+}_{1.65}Fe^{2+}_{2.38}Mg_{1.48})_{5.51}$

* 3% of feldspar should be added

14-HL 18 and 7-BG 15 are characterized by a high heterogeneity of octahedral cation composition (Table 4). In sample 14-HL 18 the amount of Al is slightly higher than that of (Fe^{3+}+Fe^{2+}) whereas the cation composition of sample 7-BG 15 contains a significant amount of Mg.

Random powder XRD patterns

Table 5 compares d_{hkl} and *hkl* reflections published for berthierine and odinite (Bailey, 1988) with those determined for samples 10-HL 7 and 16-HL 24 based on their random powder XRD patterns. These data show that, as in the case of berthierine and odinite, both samples contain a physical mixture of orthogonal and monoclinic varieties of a berthierine-like mineral, since their XRD patterns contain *hkl* reflections corresponding to these polytypic phases. The parameters of the orthogonal and monoclinic unit-cells are similar in both samples and are equal to: a = 5.390 Å, b = 9.330 Å, c = 7.13 Å for the orthogonal and a = 5.390 Å, b = 9.330 Å, c = 7.365 Å, β = 104.5º for the monoclinic unit-cells. The values of d_{hkl} calculated for these cells and shown in the last column of Table 5 coincide within experimental error with the experimental d_{hkl} values. The comparison of the parameters with those found for odinite and berthierine shows that both polytype modifications have the same, or quite similar, lateral dimensions, whereas the c and $c$sinβ parameters for the orthogonal and monoclinic modifications in the studied samples (7.13 Å) are intermediate between those determined for berthierine (7.04 Å) and odinite (7.15 Å) (Bailey, 1988).

Figure 9 shows the 060 regions in the powder XRD patterns of the studied samples. The observed intensity modulations in these regions can be interpreted using the computer simulations in combination with the weighted concentrations and averaged formulae of the layer types present in the samples (Table 4) and FTIR data (Figure 4). The region from samples 7-BG 15 and 14-HL 18 contains one asymmetrical maximum at 1.515 Å corresponding to the 060 reflection of glauconite. Taking into account that these samples are practically monomineralic, the asymmetrical shape of the reflection is associated with the octahedral cation heterogeneity of individual glauconite particles. Particles where Fe^{3+} cations prevail coexist with those containing a significant amount of octahedral Al. This conclusion is in agreement with the heterogeneous octahedral cation composition shown in the structural formulae of the samples (Table 4) and with the IR spectra which show a significant contribution of Al-OH-Al and Al-OH-Mg cationic pairs.

The 060 region from samples 5-BG 7 and 21-LGB 7 contains one maximum at 1.544–1.547 Å corresponding to trioctahedral chlorite. The other 060 maximum at 1.504–1.507 Å should correspond to Fe^{3+}-bearing I-S, whereas asymmetrical shape and broadening of the maximum are caused by contribution of illite (at 1.50 Å), kaolinite (1.49 Å), and K-S-V. The contribution of the last phase should probably be at 1.495 Å if a

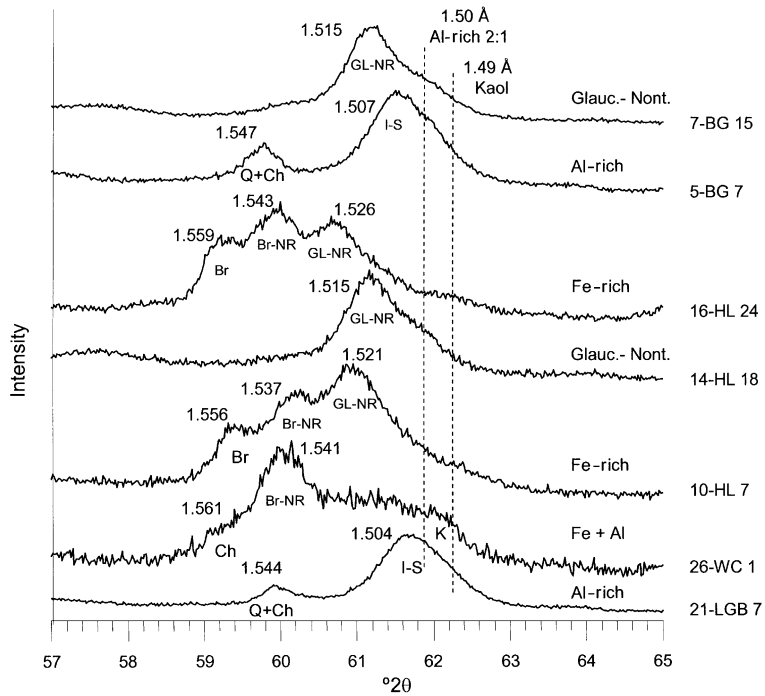

Figure 9. Diffraction patterns of the 060 region (see text) for random powders (<2 μm) . GL-NR = glauconite-nontronite, I-S = illite-smectite, Br-NR = berthierine-nontronite, Q = quartz, Ch = chlorite, Kaol = kaolinite, Br = berthierine-like.

https://doi.org/10.1346/CCMN.2004.0520503 Published online by Cambridge University Press

mutual adjustment of the interstratified layers lateral dimensions took place.

The 060 region of samples 10-HL 7 and 16-HL 24 has a more complex shape which consists of three modulated maxima (Figure 9). The reflections at 1.556 and 1.559 Å correspond to a discrete berthierine-like mineral as it follows from the indexing of the powder XRD patterns of samples 10-HL 7 and 16-HL 24 (Table 5). The origin of the maxima at 1.537 and 1.543 Å and at 1.521 and 1.526 Å is not so clear because at least two alternative interpretations are possible. One of the plausible interpretations is that the reflections at 1.537 and 1.543 Å are associated with the Br-NR-V phase in sample 10-HL 7 and Br-NR-Ch phase in sample 16-HL 24 whereas the maxima at 1.521 and 1.526 Å correspond to the GL-NR-V. A weak point of this interpretation is that the strong intensity of the last two reflections is not completely consistent with the relatively low concentration of the GL-NR-V in sample 16-HL 24 (7%). An alternative interpretation is the assumption that reflections at 1.521 Å and 1.526 Å are associated with glauconite-nontronite-vermiculite layers in the GL-NR-V and Br-NR-V or Br-NR-Ch, whereas reflections at 1.537 and 1.543 Å are associated only with Br layers in the Br-NR-V and Br and Ch-layers in the Br-NR-Ch. This interpretation is in agreement with total weight concentrations of GL, NR and V layers (43% *vs.* 31%) and the Br layers in the Br-NR-V (25 *vs.* 34%) and the intensity of the 060 reflections in the compared samples. Indeed, in sample 10-HL 7, the intensity of the maximum at 1.521 Å is stronger than that at 1.537 Å as well as the total amount of GL, NR and V layers (43%) being higher than the content of BR layers (25%) in the mixed-layer phase. In contrast, intensity of the

Table 5. Experimental spacings determined for berthierine, odinite (Bailey, 1988) and for samples 10-HL-7 and 16-HL 24 (this study) compared with those calculated for the orthogonal and monoclinic unit-cells; *hkl* indices are given for both modifications. The last column contains d_{hkl} values calculated for the monoclinic and orthogonal unit-cell parameters determined for sample 16-HL 24 and given in the text.

Berthierine					Odinite	This study		
Monoclinic			Orthogonal			16-HL 24	10-HL 7	
d_{calc}	*hkl*	$d_{obs.}$	d_{calc}	*hkl*	d_{calc}	d_{obs}	d_{obs}	$d_{hkl(calc)}$
7.040	001	7.05	7.04	001	7.14–7.16	7.13	7.13	7.13
4.666	020	4.67	4.666	020	4.66–4.67	~4.67	~4.68	4.667
4.568	110	4.58			4.55	4.58	4.56	4.555
4.282	111	4.28				4.29	~4.30	4.286
3.887	021	3.90	3.887	021		~3.90	~3.92	3.904
3.520	002	3.52	3.520	002	3.57–3.58	3.565	3.565	3.565
2.810	022	2.801	2.807	022		2.80		2.833
2.684	$20\bar{1}$	2.678	2.693	200	2.66–2.69	2.68	2.67	2.676
2.674	130							
		2.519	2.516	201	2.51–2.52	2.52	2.53	2.521
2.410	$20\bar{2}$	2.404			2.40–2.41	2.42	2.41	2.41
2.401								
		2.337						
2.275	201	2.273			2.28	2.28		2.274
2.274	$13\bar{2}$							
		2.141	2.139	202	2.15	2.15	2.16	2.15
2.016	$20\bar{3}$	2.011				2.03	2.03	2.027
2.009	132				2.02			
1.902	$13\bar{3}$	1.894						
1.888	202				1.9			
		1.768	1.769	203		1.782	1.78	1.782
		1.693	1.71	241		1.719		1.713
1.667	$20\bar{4}$	1.665			1.67–1.68			
1.661	133							
1.565	$13\bar{4}$	1.555	1.555	060	1.551–1.556	1.559	1.556	1.558
1.555	$33\bar{4}$; 060							
1.523	330	1.521	1.519	061	1.517	1.543	1.537	1.526
1.519	061					1.526	1.521	
		1.473	1.473	204				
1.425	331							
1.423	062	1.425	1.423	062	1.42–1.43			
1.408	005							
		1.361						
1.346	$26\bar{1}$	1.347	1.347	400				
		1.326	1.323	401				

https://doi.org/10.1346/CCMN.2004.0520503 Published online by Cambridge University Press

maxima at 1.526 Å and 1.543 Å for sample 16-HL 24 are similar to each other and the total content of the swelling layers (31%) is almost equal to the amount of Br and Ch layers (34%) in the mixed-layer phase (Table 4).

The 060 region of sample 26-WC 1 reflects its intermediate clay composition with some characteristics similar to the Fe-rich samples 10-HL 7 and 16-HL 24 and others to more aluminous samples 5-BG 7 and 21-LGB 7. It is likely that the strong reflections at 1.541 Å correspond to trioctahedral chlorite and the Br-NR-V or berthierine layers in this phase. A broad band between 1.530 and 1.500 Å reflects a wide octahedral cation diversity in 2:1 layers in the NR-Br-V and Br-NR-V. Significant intensity from 1.50 to 1.485 Å corresponds to the 060 reflection of kaolinite.

Stratigraphic relationships

Based on all of the above structural and compositional data from these seven samples, the diffraction patterns from all of the <2 μm preparations from the five stratigraphic groups can be categorized according to their similarity to one of these seven samples. Thus, the clay assemblages can be classified as being (1) Al-rich, consisting of I-S-V and K-S-V and some amount of discrete illite (15−25%) and of kaolinite (5−7%), like samples 5-BG 7 and 21-LGB 7; (2) Fe-rich, with the presence of discrete berthierine-like phase, Br-NR-V and GL-NR-V, like samples 10-HL 7 and 16-HL 24; (3) samples which are mostly pure glauconite or nontronite-like samples 7-BG 15 and 14-HL 18; and (4) those samples that have intermediate Fe and Al clay compositions like 26-WC 1.

In general, clays from the Blackgang interval are dominated by the Al-rich category, especially the I-S such as may be derived from bentonitic material. An exception is the 7-BG 15 sample that is glauconite with an impurity of pure nontronite and 8-BG 16 (Table 1, Figure 2) in which nontronite is the main phase. The Horse Ledge clays are dominated by Fe-rich 2:1 and 1:1 layer clays, but with two intermediate samples and two glauconitic-nontronitic (GL-NR) samples. The Whale Chine samples are characterized by mostly intermediate (Fe + Al) to Al-rich clays, but with two GL-NR samples. The Lower Gryphea Bed–Barnes High samples are characterized by intermediate to Al-rich clays with two intervening GL-NR samples (Figure 2).

DISCUSSION

Reliability of structural and probability parameters of the studied minerals

The conventional approach of using peak positions and comparing diffraction patterns from air-dried and EG preparations to interpret the mixed-layer structures in multiphase samples is of limited use. By this approach it is difficult to determine the presence of high-charge smectite or vermiculite layers in I-S and GL-NR as well as to identify other types of mixed-layer phases containing, along with expandable layers, kaolinite, serpentine and chlorite layers. Similarly, it is difficult to distinguish Fe-rich from Al-rich layers.

The results obtained in this work show that computer simulation is one of the best ways to provide a reliable interpretation of the experimental XRD patterns and accurate determination of structural and probability parameters of the minerals in the Isle of Wight samples. Satisfactory agreement between positions, intensities and profiles of basal reflections in calculated and experimental XRD patterns reveals coexistence in the same sample of up to three mixed-layer phases, each of which consists of three types of layers having different thicknesses, cation compositions, contents and distributions. Among these mixed-layer phases, Br-NR-V and especially Br-NR-Ch have probably not been described in the literature.

The reliability of structural and probability parameters of the studied mixed-layer phases is confirmed by the fact that satisfactory agreement between the experimental and calculated XRD patterns was obtained for specimens of the same sample in air-dried and EG states using the same statistical model (Tables 3, 4).

A significant advantage of the approach is that it provides quantitative phase analysis of the samples containing periodic and interstratified clay minerals (Table 3). The average cation composition of the layer types in each of the studied samples were determined by partitioning the total sample oxide contents (Table 4) based on the relative weighted concentrations of the particular layer types determined from computer simulation (Table 3).

The more discrete and mixed-layer phases that coexist in a sample, the more independent structural and probability parameters should be used for simulation. As a result, the reliability and accuracy in determining these parameters decreases. The presence of each particular phase in a sample is justified if this phase is responsible for certain parts of the experimental XRD pattern that do not overlap with the contributions of the other coexisting phases.

Therefore, if the agreement achieved relies on a significant increase of adjacent parameters then the actual presence of each of the mixed-layer phases needs to be assessed. The respective contributions of the GL-NR-V, Br-NR-V and NR-V-Br phases to the diffracted intensity are shown for sample 10-HL 7 in Figure 10 which compares the experimental XRD pattern with those calculated for models similar to the optimal one from which one of the contributions is systematically subtracted. As a result of these structural modifications, the quality of fit becomes systematically worse in specific parts of the calculated XRD pattern for which the subtracted phase is responsible, supporting the actual existence of each of these phases.

https://doi.org/10.1346/CCMN.2004.0520503 Published online by Cambridge University Press

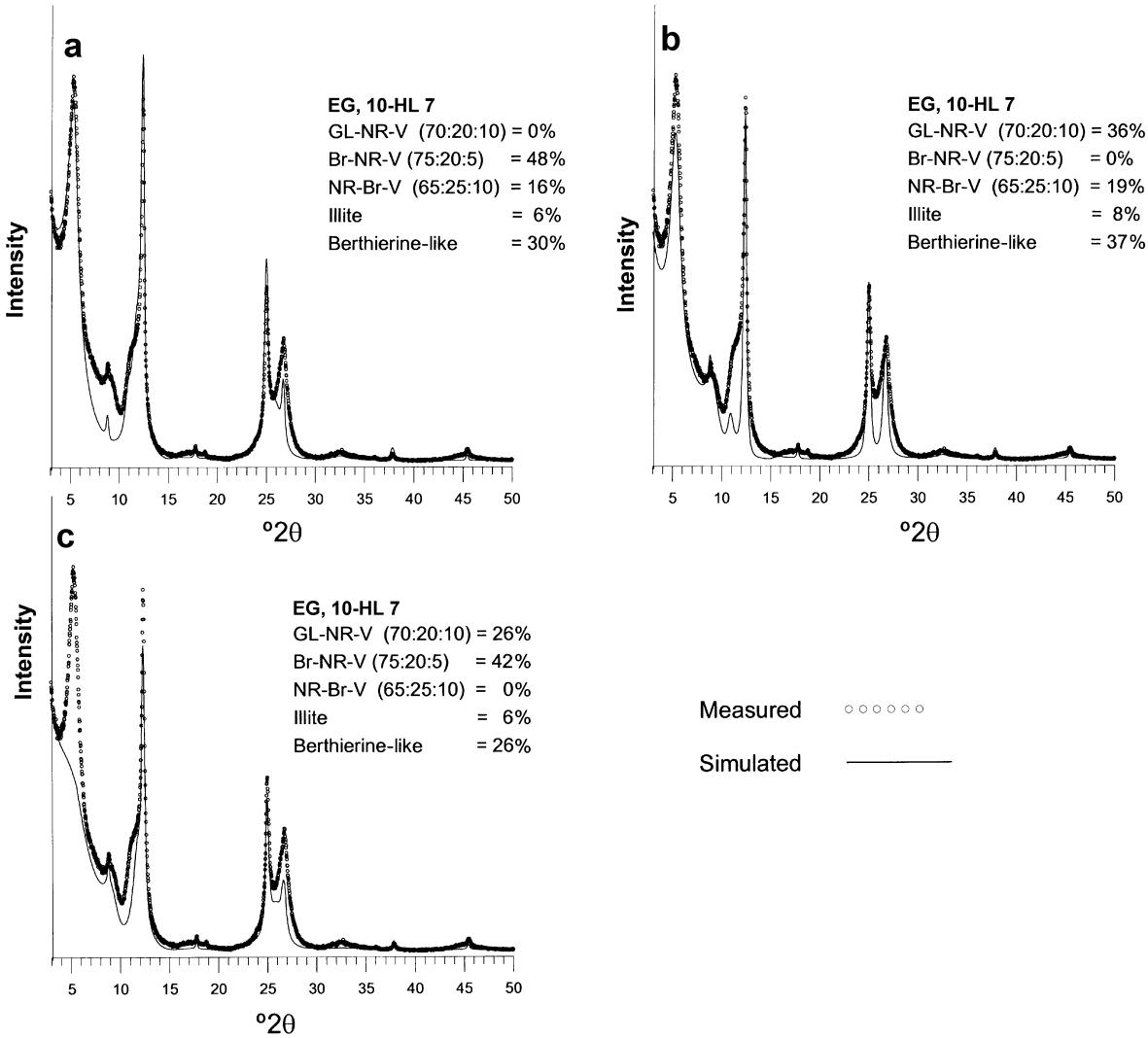

Figure 10. (a) XRD patterns from sample 10-HL-7; compared to simulated diffraction patterns without the contribution of GL-NR-V, (b) compared to simulation less Br-NR-V, and (c) less NR-Br-V, to show the respective intensity contributions to the fit solution shown in Figure 8b.

One of the remarkable features of XRD is its ability to extract average structural characteristics of crystals deprived of 3D periodicity. At the same time, this ability provides relatively low sensitivity of diffraction to local structural disorders (Drits, 1987; 1997, 2003). For this reason, the actual structure of mixed-layer phases is not always determined unambiguously because several structural models may fit the experimental XRD patterns equally well (Sakharov *et al.*, 1999; Drits *et al.*, 2002; Drits, 1997). To illustrate, Figure 6c–d compares the experimental XRD pattern of sample 5-BG 7 with that calculated for a model that consists of I-S (38%), Br-NR-V (11%) and also kaolinite (9%), illite (32%) and chlorite (10%). The quality of the fit is comparable with that obtained for a model consisting of I-S (26%), K-S-V (35%), kaolinite (7%), illite (24%) and chlorite (8%) (Figure 6a–b). Thus, replacement of K-S-V for Br-NR-V having the same amount of expandable layers but quite different layer cation compositions does not significantly modify the calculated patterns when the contents of the coexisting phases were changed dramatically.

The actual model was chosen taking into account that, according to the IR spectrum (Figure 4) and acid treatment (Figure 3), K-S-V is one of the dominant phases. This example shows that to provide reliable interpretation of XRD patterns from samples of complex phase and chemical compositions, application of different techniques as well as different sample treatments is required.

Origin of phases in Al-rich samples

The Al-rich samples along with discrete illite, smectite, kaolinite and chlorite consist of two dominant mixed-layer I-S and K-S-V phases. It is likely that illite and chlorite are detrital whereas the I-S in these samples is probably authigenic clay produced by illitization. It is

https://doi.org/10.1346/CCMN.2004.0520503 Published online by Cambridge University Press

similar to I-S found in the Gulf Coast Basin that is assumed to have a bentonitic origin. The unusual structural feature of the I-S is that interstratification of 60% I and 40% S layers occurred with some tendency to segregation at R = 1. In the literature, interstratification of I and S layers in authigenic I-S having bentonitic origin was usually described as random (R = 0) or having a tendency to order (R = 1). The whole-rock mineralogy of Al-rich samples has a significant amount of plagioclase feldspar (9–13%) and 2:1 Al clays + mica (35–48%) (Table 1), which is consistent with volcanic-derived sediment. The presence of pure smectite in some Al-rich samples can also be considered as a product of volcanic or bentonitic origin.

It is likely that the K-S-V was formed from weathering in the outcrop or by some other process providing partial transformation of smectite layers into kaolinite ones in slightly acidic conditions. For example, Shultz *et al.* (1971) described K-S from marine Tertiary clays located in the Yucatan Peninsula, Mexico. They assumed that the parent material for the K-S was a volcanic ash that was subjected to weathering in acid conditions with the formation of intermediate Al-H-montmorillonite which was in turn transformed into the K-S. This phase was transported and buried to shallow marine environments (littoral). When the acid solution changed to slightly alkaline, the kaolinization process was interrupted. The K-S-V found in the Al-rich samples may have similar history.

Crystal-chemical features and formation conditions of the berthierine-like mineral

The relationship between berthierine, odinite and glauconite has interesting and important implications for environments of formation and local geochemical conditions. For this reason it is important to know the crystal chemistry of the 1:1 layers that we call berthierine-like. Bailey (1988) described the structural and compositional differences between berthierine and odinite and summarized some of the environmental conditions where they and the glauconite facies form. Briefly, odinite and/or berthierine seem to form in shallow marine water (~15–60 m) near rivers carrying Fe in solution, whereas glaucony forms deeper (>150 m). Odinite forms authigenically in ~25ºC at pH 7.5 to 8.5 in sandy sediment that often has significant bioclastics in micro-reducing environments including infillings and replacement of detrital organic matter and pellets. Odinite alters to chlorite I*ba* and it is not yet recognized in rocks older than Recent–Quaternary (Bailey, 1988).

The idealized general berthierine formula may be described as:

$$[(Fe^{2+}Mg)_a(AlFe^{3+})_b\square_c](Si_{4-x}Al_x)O_{10}\ (OH)_8 \qquad (a)$$

where: $a + b = 5.6 - 6.0$, $b - x = 2c$, $Fe^{2+} > Mg$, $Al > Fe^{3+}$, and $(Mg, Fe^{2+}) = 2.66$ to 3.68 (Bailey, 1988).

The idealized general formula for odinite is:

$$[(Fe^{2+}Mg)_{2.10}(AlFe^{3+})_{2.70}\square_{1.20}](Si_{3.70}Al_{0.30})O_{10}(OH)_8 \qquad (b)$$

where $Fe^{3+}>Al$, $Mg>Fe^{2+}$ and Fe + Mg can be $\leqslant 5.0$ (Bailey, 1988). In berthierine, ferrous Fe is usually greater than ferric Fe and in odinite ferric Fe is much greater than ferrous Fe. Berthierine is close to completely trioctahedral, while odinite is di-trioctahedral.

In sample 10-HL 7, the average structural formula for the Br layers (Table 4) is:

$$(Fe^{3+}_{1.79}Al^{3+}_{0.56}Fe^{2+}_{2.12}Mg^{2+}_{0.79})_{5.26}(Si_{3.15}Al_{0.85})O_{10}(OH)_8 \qquad (c)$$

This crystal chemistry is intermediate between odinite and berthierine. In particular, the total sum of octahedral cations (5.26) is larger than that in odinite ($\leqslant 5.0$) but lower in berthierine (>5.6). However, the limiting case is that sample 10-HL 7 has 2.12 atoms of divalent Fe which precludes calling the structure odinite. The structural formula (c) reflects average cation composition of berthierine layers in both discrete berthierine and in the Br-NR-V phases composing sample 10-HL 7. Analysis of the 060 reflection positions of the sample (Figure 9) shows that berthierine layers in the Br-NR-V and in discrete berthierine have different d_{060} values reflecting different lateral layer dimensions. The *a b* parameters of their unit-cells are equal to 5.390 Å, 9.336 Å and 5.324 Å, 9.222 Å, respectively, for berthierine and berthierine layers in the Br-NR-V. It is plausible that this difference results from different cation compositions of the layers. In particular, it seems likely that in contrast to discrete berthierine the berthierine layers in the Br-NR-V should have smaller contents of octahedral Fe^{2+} and tetrahedral Al. The weighted concentrations of berthierine layers in discrete berthierine and in both Br-NR-V phases in the sample are equal to 23% and 25%, respectively. In this proportion the formula (c) may be split, for example, to the formulae

$$(Si_{3.0}Al_{1.0})(Al_{0.70}Fe^{3+}_{1.22}Mg_{1.02}Fe^{2+}_{2.60})_{5.54}O_{10}(OH)_8, \text{ and}$$
$$(Si_{3.24}Al_{0.76})(Al_{0.43}Fe^{3+}_{2.32}Mg_{0.56}Fe^{2+}_{1.67})_{4.98}O_{10}(OH)_8$$

corresponding to discrete berthierine and berthierine layers in the Br-NR-V, respectively. The significantly higher total amount of octahedral cations, divalent Mg and Fe^{2+} as well as tetrahedral Al in the first formula in comparison with those in the second should be associated with higher lateral layer dimensions in the discrete berthierine structure. However, there are a lot of other possible redistributions of cations in both components preserving the same average composition and the weighted proportions. Therefore, the actual cation composition of discrete berthierine and berthierine layers in the Br-NR-V remains unknown.

Table 4 shows that structural formulae determined for the berthierine-like layers in samples 26-WC 1 and 16-HL 24 are similar to that of sample 10-HL 7: the total sum of octahedral cations is equal to 5.37–5.55 and content of divalent Fe cations varies from 2.15 to 2.22.

https://doi.org/10.1346/CCMN.2004.0520503 Published online by Cambridge University Press

Thus a remarkable feature of the berthierine-like phase as well as Br layers is that they are di-trioctahedral and both Fe^{3+} and Fe^{2+} are prevailing cations. We therefore call it berthierine-like even though it is different from other published berthierine compositions (Brindley, 1982; Bailey, 1988; Toth and Fritz, 1997a).

Toth and Fritz (1997b) stated that the qualitative conditions for pure Fe^{2+}-berthierine to precipitate from solution are that it must be reducing, be low in sulfate or pyrite formation will be a sink for Fe, not be in contact with quartz, and there must be a low Mg^{2+}/Fe^{3+} ratio. These authors concluded that pure Fe-berthierine would not form in marine sediments or in sediments influenced by marine water. This is consistent with the observation that many berthierines and odinites having significant Al^{3+} and Mg^{2+} are found in shallow marine waters near rivers (Bailey, 1988). Also, it is likely that conditions in the rock or sediment pore system, including biological activity, could modify the general geochemical conditions for direct berthierine precipitation or solid-state reactions with other materials.

Possible structural mechanisms of the Br-NR-V and Br-NR-Ch formation

The high Fe^{2+} content in the average structural formulae for berthierine and chlorite layers in the Br-V-BR and Br-NR-Ch (Table 4) of samples 10-HL 7 and 16-HL 24 shows that these authigenic phases were formed in reducing or micro-reducing conditions. Several alternative assumptions concerning structural mechanisms of the Br-NR-V and Br-NR-Ch formation can be considered.

One of them consists of solid-state transformation of K-S-V into Br-NR-V by substitution of octahedral Al in the 1:1 and 2:1 layers of the first phase by Fe and Mg. For example, the comparison of phase compositions of samples 5-BG 7, 21-LGB 7 and 10-HL 7 shows that the main difference between them is that the K-S-V in the first and second samples is represented by the Br-NR-V in the third one, *i.e.* Al-rich 2:1 and 1:1 layers are replaced by Fe-rich ones. The weighted contents of the K-S-V and Br-NR-V are almost identical for these samples (33–35%, Table 3). The same weighted concentrations (25%) were determined for the I-S-V and GL-NR-V in samples 5-BG 7 and 10-HL 7. Moreover, the K-S-V and Br-NR-V in samples 5-BG 7 and 10-HL 7 contain the same amount of expandable and non-expandable layers (Table 3). Taking into account that sample 5-BG 7 contains discrete kaolinite and 10-HL 7, discrete berthierine, the formation of the mixed-layer minerals in 10-HL 7 could be a simple replacement of Al by Fe and Mg in the octahedral sheets of the 2:1 and 1:1 layers. This reaction modified neither the contents nor the mode of the layer types and their interstratification. Both samples 5-BG 7 and 10-HL 7 have high total clay, equal to 50 and 58 wt.%, respectively.

Textural features of sample 10-HL 7 under low magnification are relatively typical for mudstone or shale texture (Figure 11a). However, the clays themselves of the sample have an authigenic texture under high magnification (Figure 11b) suggesting that they were formed by transformation of the detrital Al-rich clay minerals among which mixed-layer K-S-V prevailed. It is plausible that K-S-V particles are more reactive than discrete kaolinite. This assumption may explain the phase composition of sample 26-WC 1 in which, along with discrete kaolinite, illite and Mg-rich chlorite, the Br-NR-V is present. In this phase the contents of berthierine and expandable layers (0.70 *vs.* 0.30) are similar to those determined for the K-S-V in samples 21-LGB 7 (0.70 *vs.* 0.30) and 5-BG 7 (0.75 *vs.* 0.25), that is the Br-Nr-V was perhaps formed due to replacement of Al for Fe and Mg in the K-S-V.

Odinite as well as berthierine may be altered to chlorite and this reaction may occur as a solid-phase transformation of two adjacent berthierine layers into a chlorite layer by the inversion of the tetrahedral sheet in one of the 1:1 layers (Bailey, 1988; Bailey *et al*. 1995). A similar reaction probably took place to transform the Br-NR-V into Br-NR-Ch. Indeed, there is a close relationship between the probability parameters describing the amount of the interstratified layers in the Br-NR-Ch of sample 16-HL 24 and Br-NR-V in samples 10HL 7 and 26-WC 1. Let us assume that 0.45 of the total amount of berthierine layers in the Br-NR-V (75%) was transformed into 16.9% chlorite layers. Then the average contents of chlorite, berthierine and nontronite layers in the particles of the transformed phase should be equal to 16.9, 41.2 and 25%, respectively. After normalization, the new-formed Br-Ch-NR should contain 50% berthierine, 20% chlorite and 30% nontronite layers. These values almost coincide with those (50, 20 and 30%) which are characteristic of Br-Ch-NR in sample 16-HL 24 (Table 3). The strong point of this hypothesis is that first, the Br-NR-V inherits the character of the K-S-V and, what is more important, the contents of the 2:1 and 1:1 layers; and, second, the Br-NR-Ch inherits the structural features of the Br-NR-V if the solid-phase transformation of the berthierine-like layers into chlorite ones took place.

However, SEM images of the clay separation from sample 16-HL 24 (Figure 11c–d) show a typical smectitic texture that differs from that observed for sample 10-HL 7 (Figure 11a–b). Therefore, the alternative hypothesis for the origin of the mixed-layer phases is that an intermediate Fe^{3+}-rich nontronite was initially formed, which in turn was transformed into the mixed-layer phases. We may assume that the transformation of Fe^{3+}-rich 2:1 layers into Fe^{2+}, Mg-rich 1:1 layers took place within the initial smectite matrix in micro-reducing environments which could be related to biological activity. Reduction of Fe^{3+} cations in the nontronite layers should disturb their stability because of the charge imbalance. This imbalance cannot be compensated by sorption of protons because they are absent even in slightly alkaline solutions. The reducing reaction probably serves as a trigger for the

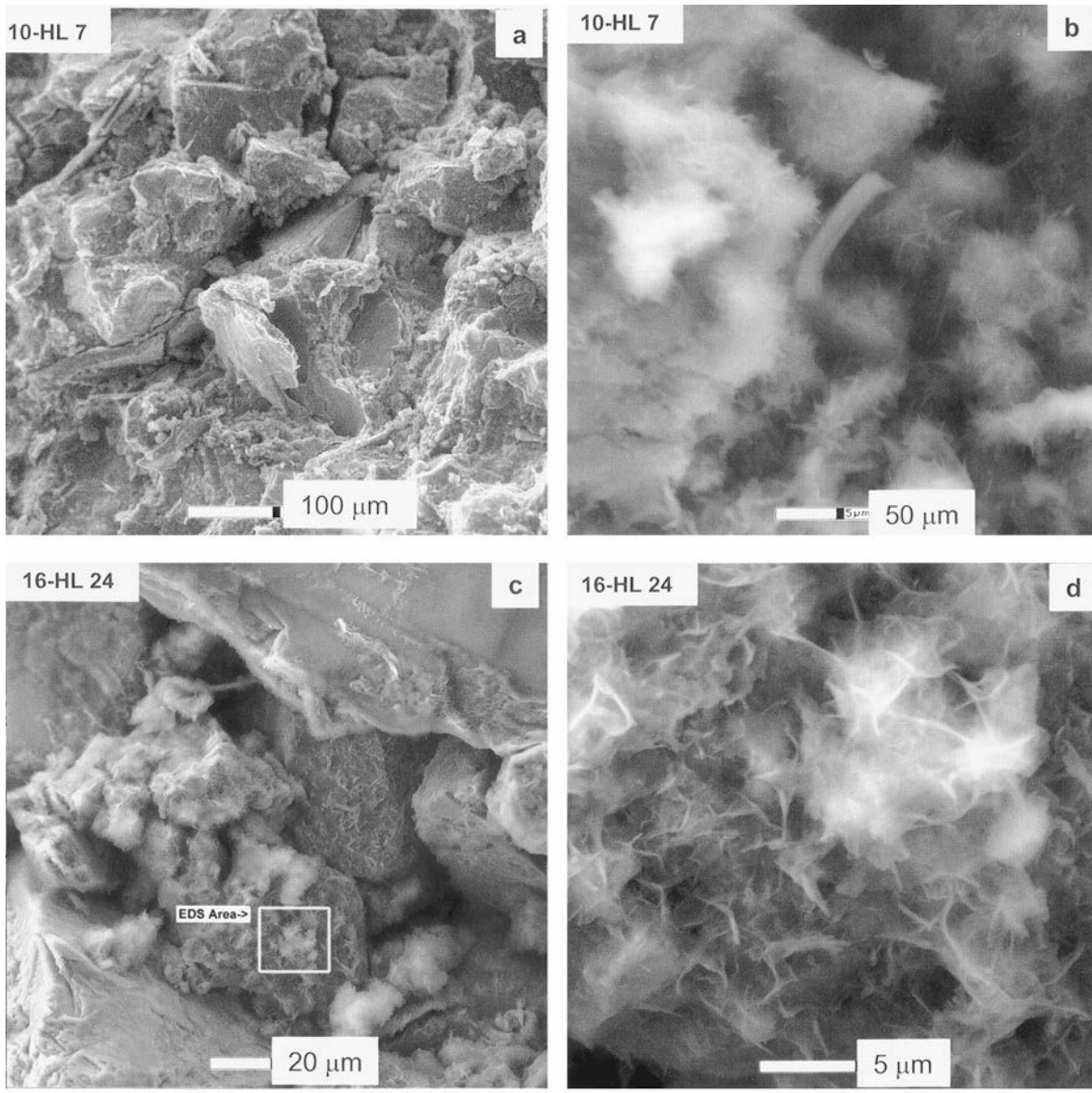

Figure 11. SEM images: sample 10-HL 7 showing detrital mudstone fabric (a); and authigenic clay texture at high magnifications (b); sample 16-HL 24 showing clay coatings on quartz grains (c); and authigenic smectitic texture at high magnification (d).

transformation of the nontronite layers into berthierine-like ones. Such a transformation should take place only within some individual 2:1 layers preserving other layers from reaction. It seems unlikely that a Br-NR-V phase in which Fe^{3+}-rich 2:1 layers coexist with Fe^{2+}-rich 1:1 layers could be formed by a direct crystallization from solution.

Further investigations are needed to reveal the actual structural mechanism and environmental conditions of Br-NR-V and Br-NR-Ch formation.

Glauconite-nontronite relationships

Regardless of the prevailing category of clay there are intervening samples in the section that are characterized by glauconite and nontronite. The major mineral components (Table 1) are displayed in Figure 12 and the samples where glauconite and/or nontronite are the main clay mineral in the <2 μm fraction are shown. It is striking that wherever such clays occur, both K-feldspar and plagioclase are absent.

According to Odin (1988) the glaucony facies forms near the sediment-water interface and it forms best (often exclusively) in granular sediment. Crystal growth starts in pores, which may extend across grains. Evolution of glaucony or the glauconitization of nontronite (*i.e.* to high K_2O ~8 wt.%) may be halted if the environment becomes unstable. Odin (1988) considers the main factors are (1) regressive sea level, causing a

https://doi.org/10.1346/CCMN.2004.0520503 Published online by Cambridge University Press

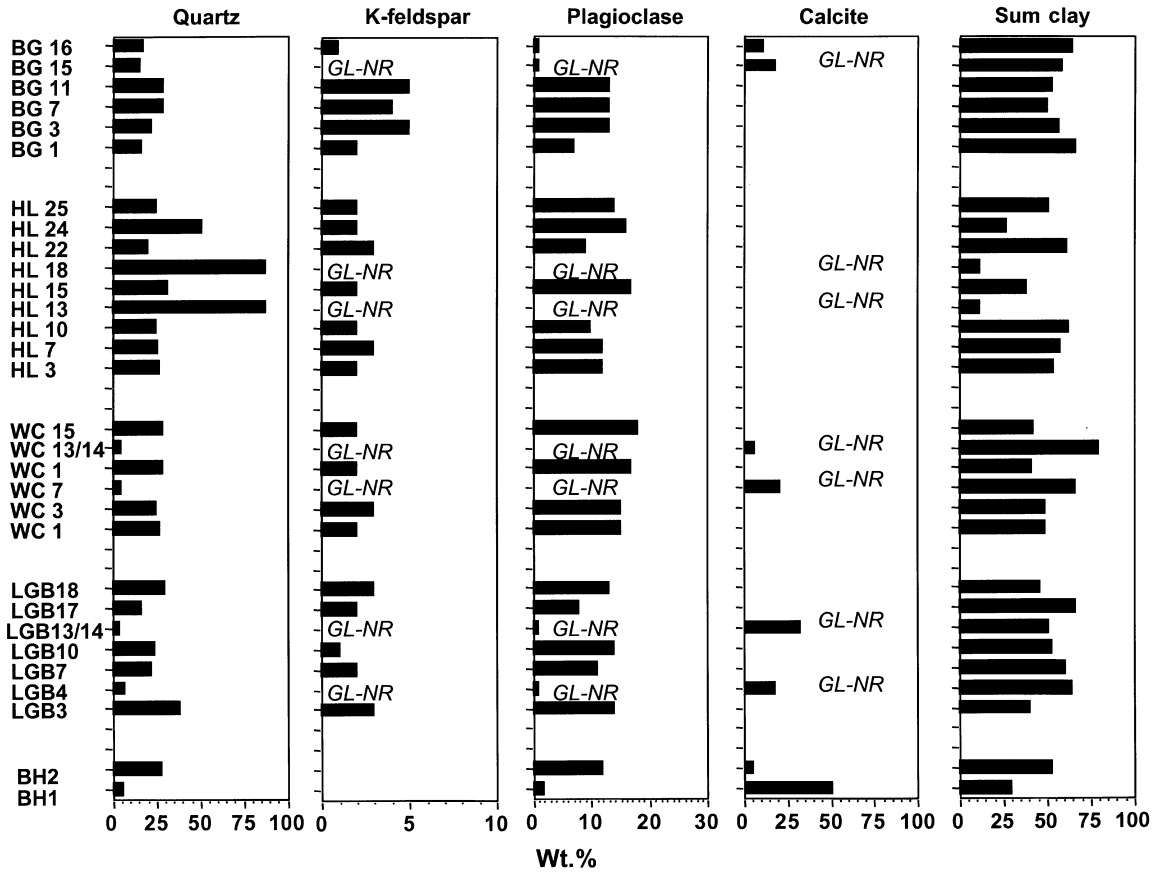

Figure 12. Whole-rock mineralogy of Isle of Wight samples showing that those which contain only glauconite-nontronite in the <2 μm oriented preparations correspond to whole-rock samples that do not contain K-feldspar and plagioclase.

more oxidizing environment, (2) a transgressive sea level causing phosphatization, and (3) burial. Burial below ~1 m may halt the process.

Abundant plagioclase, K-feldspar and Al-rich 2:1 layer clays and mica in the bulk rock suggest a volcanic or volcanoclastic origin of the sediment. The fact that glauconite and nontronite only occur when feldspar is absent suggests that volcanism or volcanoclastic sedimentation was the process that completely inhibited glauconite-nontronite formation in the other Isle of Wight samples that do not contain GL-NR as the dominant clay phase. It is doubtful that K-feldspar and plagioclase are absent because they were consumed as a reactant in glauconitization because the glauconite-nontronite association occurs exclusively when both K- and plagioclase feldspar are absent, and there is no explanation for the lack of plagioclase in such samples except that it was not deposited with the original sediment. Volcanic deposits are recognized in the Cretaceous section (Ruffell *et al*., 2002) and the tectonic setting in the region was conducive to volcanic activity (Roberts *et al*., 1999). Many other papers describe 'episodic' periods of volcanic sedimentation during the depositional time period of the section studied here. Some authors discuss the regional distribution of volcanoes (Bennet *et al*., 1985; Larson, 1991), while others document bentonites in specific areas (Goldring, 1999; Hallam and Sellwood, 1968; Jeans *et al*., 1977; 1982: Wray and Wood, 1998; Young *et al*., 1978; and Zimmerle, 1979). Together, these show the widespread distribution of Aptian volcanoes and their products.

Furthermore, if sea-level change or bioturbation alone were responsible for creating an unstable substrate to prevent formation of glauconite-nontronite clay and glauconitization, then you would not expect glauconite-nontronite to be found in samples exclusively lacking feldspar. After initial nontronite growth during times of low volcanoclastic deposition, the substrate may again become less stable by other factors (Odin, 1988) and inhibit the evolution of nontronite to glauconite.

Intensity of glauconitization was different for different samples reflecting variable sedimentation conditions. For example, the most evolved glauconitic clay, in sample 14-HL 18 (Figure 5), essentially consists of only quartz (88 wt.%) and 2:1 Fe-rich clay (11 wt.%) (Table 1). Analysis by SEM shows that this well crystallized GL-NR exists as fine coatings on the quartz grains (Figure 13a). No discrete pellets or clay globules were observed in this sample.

In contrast, sample 7-Bg 15 along with the GL-NR-V contains discrete nontronite (3%) (Figure 5b) and has

https://doi.org/10.1346/CCMN.2004.0520503 Published online by Cambridge University Press

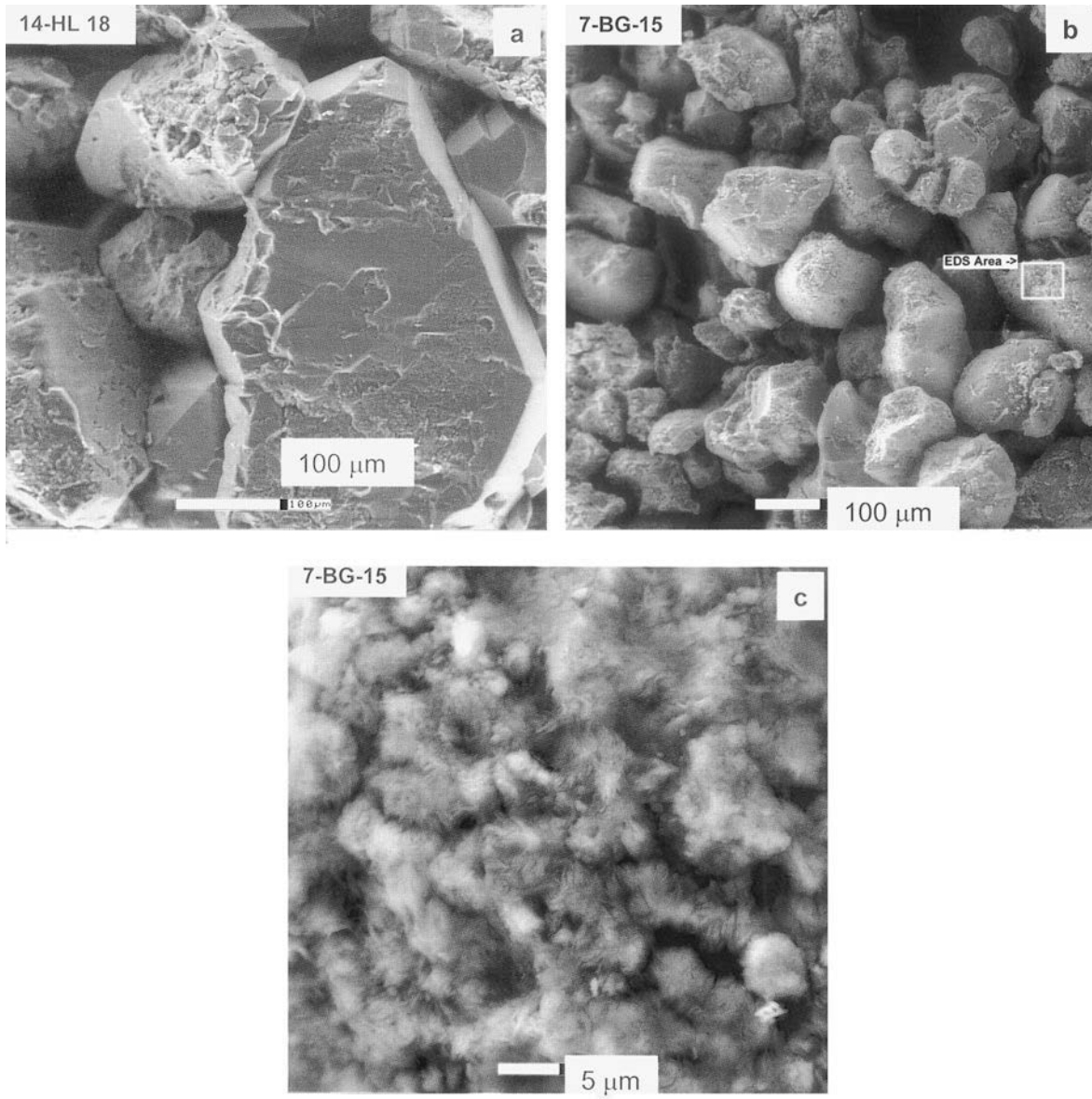

Figure 13. SEM images: sample 14-HL-18, that with the most evolved glauconite, exists as a finely dispersed coating on quartz grains (a). Sample 7-BG-15 with less evolved glauconite-nontronite grew more abundantly as grain coatings (b,c).

higher total clay (59 wt.%, Table 1). The evolution of this sample may have resulted in complete glauconitization of a portion of the <2 μm clay, while another portion of pure nontronite remained. Perhaps this is due to biological activity of micro-environments that enable the glauconitization process to occur in only selected locations in the sediment. The phase heterogeneity of the sample shows that sedimentation conditions do affect glauconitization after the initial nontronite was formed. The GL-NR-V also grew as coatings on the grains, but is clearly more abundant and grew with a very fine or diffuse texture as seen under high SEM magnification (Figure 13b–c).

Despite differences in sedimentation conditions, individual particles or clusters within these particles in both samples are characterized by a significant heterogeneity in the isomorphous octahedral cations distribution. Structural formulae of samples 7-BG 15 and 14-HL 18 (Table 4) show that their 2:1 layers along with a significant Mg content contain comparable amounts of octahedral Al and Fe^{3+}. However, these cations are not distributed at random but have some tendency to be segregated into Fe-rich and Fe-poor particles or clusters. This conclusion follows from an intensive shoulder observed from the higher 2θ region in the 060 reflection profiles observed for both samples (Figure 9). In fact, their 060 reflection can be decomposed into two discrete maxima with d = 1.515 Å and 1.505 Å corresponding to the Fe^{3+}-rich and Fe^{3+}-poor particles or clusters. The IR

https://doi.org/10.1346/CCMN.2004.0520503 Published online by Cambridge University Press

spectra of the samples (Figure 4) also show two discrete regions in one of which the main contribution provides Al-OH-Al and Al-OH-Mg, whereas in the other Fe-OH-Fe and Fe-OH-Mg cationic pairs. These diffraction and spectroscopic features can be explained by coexistence of clusters or particles containing different amounts of Al and Fe^{3+}. The coexistence of clays with a glauconite, Fe-illite and illite cation composition in the same sample or even in the same granular globule particles was documented for glauconite samples of different age and location by Tsipursky *et al*. (1992), Shutov *et al*. (1973), and Dupley (1988).

SUMMARY

Within <200 m, Isle of Wight clays are heterogeneous assemblages with discrete and mixed-layer clay minerals. Layers types include: illite, smectite, glauconite, nontronite, kaolinite, chlorite and a 7 Å berthierine-like structure. Mixed-layer clays coexist with different layer proportions in the same sample.

Sediment with significant GL-NR is granular as observed by Odin (1988), but not exclusively and some samples with significant nontronite have >50% total clay. However, feldspar is always absent when GL-NR is the dominant clay in the <2 μm fraction. This suggests that sedimentation from a volcanic source created an unstable substrate that was not favorable to glauconitization. Many of the clays observed in this study such as the Blackgang samples are Al-rich probably from bentonitic material. However, even within intervals such as the Al-rich Blackgang group, glauconite-nontronite clays form in feldspar-free samples suggesting that there was a lull in volcanoclastic sedimentation, creating a stable substrate favorable for initial GL-NR growth. It is possible that sea level and/or possibly bioturbation created an unstable substrate at a later time to limit the evolution of nontronite to more glauconitic clays (Odin, 1988) and/or volcanoclastic sedimentation resumed and the more expandable clays are preserved in the sample.

Berthierine-like samples have intermediate total clay and are associated with less evolved GL-NR (unstable substrate). Perhaps berthierine-like layer formation relates to micro-reducing environments, which could be related to biological activity that in some way favors formation these layers interstratified with other layer types.

The authigenic clays in the Isle of Wight samples include: glauconite and GL-NR from the glauconitization process; smectite probably from alteration of volcanic ash; mixed-layer I-S from the illitization process; a 7 Å berthierine-like structure both in mixed-layer clays and as a discrete mineral. The Fe^{2+} in this structure indicates a reducing or micro-reducing environment. The Br-NR-V and NR-V-Br phases may be formed from the K-S-V by substitution of octahedral Al in the 1:1 and 2:1 layers by Fe and Mg. The berthierine-like layers may also have somehow formed from alteration of nontronite in such conditions, or possibly from a reaction with kaolinite and Fe oxides in reducing conditions (Toth and Fritz, 1997). However, the significant Mg^{2+} content suggests some marine water influence, but perhaps not fully marine. It is interesting that more than one mixed-layer structure with berthierine-like layers coexist in the same sample.

The variation in clay types through each sediment cycle, and even within one sample of such a cycle, indicates greater mineralogical variability than would be expected, especially within the shallow marine (Ferruginous Sands, LGB, WC and HL) horizons. These samples were taken through firmground cycles (Ruffell and Wach, 1998) in which numerous episodes of deposition, erosion, faunal colonization and sea-floor cementation are documented. As such, sediment may have been buried, ingested by organisms and eroded prior to final deposition, during which time clay transformation is likely, resulting in widely varying mineralogy.

It is not obvious that kaolinite is authigenic or detrital, but a detrital origin seems reasonable. A significant amount of mixed-layer kaolinite-smectite is present in these samples and may have formed by alteration of smectite in outcrop.

ACKNOWLEDGMENTS

We are especially grateful to Russell Anderson for help with sample preparation and data collection, and Holger Lindgreen for Mössbauer analysis. The manuscript was greatly improved with reviews by Javier Cuadros, Associate Editor Crawford Elliot and an anonymous reviewer. All the authors are grateful to ChevronTexaco and RFFI for support.

REFERENCES

Bailey, S.W. (1988) Structures and compositions of other trioctahedral 1:1 phyllosilicates. Pp. 169–188 in: *Hydrous Phyllosilicates (Exclusive of Micas)* (S.W. Bailey, editor). Reviews in Mineralogy, **19**, Mineralogical Society of America, Washington, D.C.

Bailey, S.W., Banfield, J.F., Barker, W.W. and Katchan, G. (1995) Dozyite, a 1:1 regular interstratification of serpentine and chlorite. *American Mineralogist*, **80**, 65–77.

Bennet, S., Copestake, P. and Hooker, N.P. (1985). Stratigraphy of the Britoil 72/10-A Well, Western Approaches. *Proceedings of the Geologists' Association*, **96**, 225–261.

Besson, G. and Drits, V.A. (1997) Refined relationships between chemical composition of micas and their infrared spectra in the OH stretching region. *Clays and Clay Minerals*, **45**, 158–183.

Bray, R.J., Duddy, I.R. and Green, P.F. (1998) Multiple heating episodes in the Wessex Basin: implications for geological evolution and hydrocarbon generation. Pp. 199–213 in: *Development, Evolution and Petroleum Geology of the Wessex Basin* (J.R. Underhill, editor). Special Publication, **133**, Geological Society, London.

Brindley, G.W. (1982) Chemical compositions of berthierines

– A review. *Clays and Clay Minerals*, **30**, 153–155

Chung, F.H. (1974) Quantitative interpretation of X-ray diffraction patterns of mixtures. I. Matrix-flushing method for quantitative multicomponent analysis. *Journal of Applied Crystallography*, **7**, 519–525.

Drits, V.A. (1987) Mixed-layer minerals: Diffraction methods and structural features. *Proceedings of the International Clay Conference, Denver*, *1985*, pp. 33–45.

Drits, V.A. (1997) Mixed-layer minerals. Pp. 153–190 in: *Modular Aspects of Minerals* (S. Merlino, editor). EMU Notes in Mineralogy, **1**, Eötvös University Press, Budapest.

Drits, V.A. (2003) Structural and chemical heterogeneity of phyllosilicates and clay minerals. *Clay Minerals*, **38**, 403–432.

Drits, V.A., Lindgreen, H. and Salyn, A. (1997a) Determination by X-ray diffraction of content and distribution of fixed ammonium in illite-smectite. Application to North Sea illite-smectites. *American Mineralogist*, **82**, 79–87.

Drits, V.A., Sakharov, B.A., Lindgreen, H. and Salyn, A. (1997b) Sequential structure transformation of illite-smectite-vermiculite during diagenesis of Upper Jurassic shales from the North Sea and Denmark. *Clay Minerals*, **32**, 351–371.

Drits, V.A., Sakharov, B.A., Dainyak, L.G., Salyn, A.L. and Lindgreen, H. (2002) Structural and chemical heterogeneity of illite-smectite from Upper Jurassic mudstones of East Greenland related to volcanic and weathered parent rocks. *American Mineralogist*, **87**, 1590–1607.

Dupley, J. (1988) Geochimie des argiles et geothermonmetrie del populations monominerals de particles. Thesis, L'Universite' L. Pasteur, Strasbourg, France, 280 pp.

Goldring, R. (1999) Sedimentological aspects and preservation of Lower Cretaceous (Aptian) bentonites (fuller's earth) in southern England. *Neues Jahrbuch für Geologie und Palaontologie*, **214**, 3–24.

Hallam, A. and Sellwood, B.W. (1968) Origin of fuller's earth in the Mesozoic in southern England. *Nature*, **220**, 1193–1195.

Jackson, M.L. (1985) *Soil Chemical Analysis – Advanced Course.* 2nd edition. Published by the author, Madison, Wisconsin, USA.

Jeans, C.V., Merriman, R.J. and Mitchell, J.G. (1977) Origin of Middle Jurassic and Lower Cretaceous fuller's earths in England. *Clay Minerals*, **12**, 11–44.

Jeans, C.V., Merriman, R.J., Mitchell, J.G. and Bland, D.J. (1982) Volcanic clays in the Cretaceous of southern England and Northern Ireland. *Clay Minerals*, **17**, 105–156.

Farmer, V.C. (1974) The layer silicates. Pp. 331–363 in: *Infrared Spectra of Minerals* (V.C. Farmer, editor). Monograph, **4**, Mineralogical Society, London.

Larson, R.L. (1991) Latest pulse of the Earth: evidence for a mid-Cretaceous superplume. *Geology*, **19**, 547–550.

McCarty, D.K. and Reynolds, R.C. Jr. (1995) Rotationally disordered illite-smectite in Paleozoic K-bentonites. *Clays and Clay Minerals*, **43**, 271–284.

Moore, D.M. and Reynolds, R.C. Jr. (1997) *X-ray Diffraction and the Identification and Analysis of Clay Minerals*, 2nd edition. Oxford University Press, New York.

Odin, G.S. (1988) *Green Marine Clays*. Developments in Sedimentology, **45**. Elsevier, Amsterdam.

Roberts, D.G., Thompson, M., Michener, B., Hossack, J., Carmichael, S. and Bjornseth, H.M. (1999) Paleozoic to Tertiary rift and basin dynamics: Mid-Norway to the Bay of Biscay – a new context for hydrocarbon prospectivity in the deep water frontier. Pp. 7–40 in: *Proceedings of the 5th Petroleum Geology of NW Europe Conference*, London, Vol. 1, Geological Society, London.

Ruffell, A.H. and Wach, G.D. (1998) Firmgrounds – key surfaces in recognition of parasequences in the Aptian Lower Greensand Group, Isle of Wight (southern England). *Sedimentology*, **45**, 91–107.

Ruffell, A.H., Hesselbo, S.P., Wach, G.D., Wray, D.S. and Simpson, M.I. (2002) Fuller's earth (bentonite) in the Lower Cretaceous (Upper Aptian) of Shanklin (Isle of Wight, southern England). *Proceedings of the Geologists' Association*, **113**, 281–290.

Sakharov, B.A., Lindgreen, H., Salyn, A.L. and Drits, V.A. (1999) Determination of illite-smectite structures using multispecimen XRD profile fitting. *Clays and Clay Minerals*, **47**, 555–566.

Schultz, L.G., Shepard, A.O., Blackmon, P.D. and Starkey, H.C. (1971) Mixed-layer kaolinite-montmorillonite from the Yucatan Peninsula, Mexico. *Clays and Clay Minerals*, **19**, 137–150.

Shutov, V.D., Katz, M.Yu., Drits, V.A. and Sokolova, A.L. (1973) Crystallochemical heterogeneity of glauconites depending on conditions of their formation and postsedimentary changes. *Proceedings of the International Clay Conference,* Madrid, 1972, pp. 269–279.

Środoń, J., Drits, V.A., McCarty, D.K., Hsieh, J.C.C. and Eberl, D.D. (2001) Quantitative X-ray diffraction analysis of clay-bearing rocks from random preparations. *Clays and Clay Minerals*, **49**, 514–528.

Toth, T.A. and Fritz, S.J. (1997a) An Fe-berthierine from a Cretaceous laterite: Part I. Characterization. *Clays and Clay Minerals*, **45**, 564–579.

Toth, T.A. and Fritz, S.J. (1997b) An Fe-berthierine from a Cretaceous laterite: Part II. Estimation of Eh, pH and pCO_2 conditions of formation. *Clays and Clay Minerals*, **45**, 580–586.

Tsipursky, S.I., Ivanovskaya, T.A., Sakharov, B.A, Zviagina, B.B. and Drits, V.A (1992) The nature of coexistence glauconite, Fe-illite and illite in granular Fe-bearing nodules from deposits having different lithology and age. *Lithologiya I Poleznye Iscopaemye*, **5**, 65–75.

Wray, D.S. and Wood C.J. (1998) Distinction between detrital and volcanogenic clay-rich beds in Turonian-Coniacian chalks of eastern England. *Proceedings of the Yorkshire Geological Society*, **52**, 95–105.

Yoshida, S., Jackson, M. D., Johnson, H. D., Muggeridge, A.H. and Martinius, A.W. (2001) Outcrop studies of tidal sandstones for reservoir characterization (Lower Cretaceous Vectis Formation, Isle of Wight, southern England). Pp. 233– 257 in: *Sedimentary Environments Offshore Norway – Paleozoic to Recent* (O. Martinsen and T. Dreyer, editors). Norsk Petroleums-forening (Norwegian Petroleum Society; NPF), Special Publication **10**. Elsevier Science B.V., Amsterdam.

Young, B., Morgan, D.J. and Highley, D.E. (1978) New fuller's earth occurrences in the Lower Greensand of southeastern England. *Transactions of the Institution of Mining and Metallurgy*, **87**, B93–B96.

Zimmerle, W. (1979) Lower Cretaceous tuffs in northwest Germany and their geotectonic significance. *Aspekte der Kreide Europas, Journal of the Union of Geological Sciences*, Series **A6**, 285–402.

(*Received 19 December 2003; revised 19 May 2004; Ms. 868; A.E. W. Crawford Elliott*)